Lower Carboniferous igneous intrusions within the crystalline basement of the Baltic Basin (SW edge of the East European Craton, Poland) – insight based on seismic data interpretation and seismic forward modelling

Piotr Krzywiec[1], Łukasz Słonka[1], Paweł Poprawa[2]

[1]Institute of Geological Sciences, Polish Academy of Sciences Warsaw, Twarda Street 51/55, 00-818 Warsaw, Poland
[2]Faculty of Geology, Geophysics and Environmental Protection, AGH University of Krakow, 30 Mickiewicza Av., 30-059 Kraków, Poland

Correspondence to: Piotr Krzywiec (piotr.krzywiec@twarda.pan.pl)

Abstract. The deep, high-resolution regional-scale seismic profiles of the PolandSPAN® survey provided a unique insight into the extensive system of inferred igneous intrusions imaged within the crystalline basement of the Baltic Basin (SW part of the East European Craton). These intrusions, that continue laterally for 100+ km, are located at depth of c. 6-7 – 19-20 km, and are far beyond the reach of the deepest wells. They are represented by packages of strong seismic reflectors, sometimes saucer-shaped, and are often characterized by step-wise geometry, sometimes diverging into several separate branches. Forward seismic modelling was used in order to provide insight – "educated guess" - regarding their lithology, exact lateral extent, and lateral thickness variations. It was concluded that most probably these are doleritic intrusions of thickness in the range of 60 to 200 m. Due to lithological coherence and close spatial relation to shallow sills and massifs recognized in wells, they have been interpreted as Mississippian (early Carboniferous) intrusions belonging to the recently recognized Lublin-Baltic Igneous Province. Developed methodology that combines quantitative assessment of seismic data resolution and estimation of tuning thickness with 2D seismic forward modelling based on geological constrains might be used to better understand, or estimate, parameters characterizing deep intrusions that are beyond reach of deep wells.

1 Introduction

Some igneous intrusions located within the crystalline basement have been drilled by deep wells – an excellent example of this is provided by results of the Gravberg-1 and Stenberg-1 wells drilled in 1988 within the so-called Silian Ring (meteorite impact site) formed in Devonian in central Sweden (Juhlin, 1990; Papasikas and Juhlin, 1997; Juhlin et al., 2012). Both these wells were located using seismic reflection data that imaged series of high-amplitude seismic events, and they proved that these observed seismic features are related to dolerite sills hosted by granites (Juhlin, 1990; Papasikas and Juhlin, 1997). This however is not a rule, this is rather an exception as usually seismic features interpreted as deep crustal igneous intrusions are located far beyond the reach of even deepest wells (e.g. Wrona et al., 2019). In such a case, determination of their key characteristics such as lithological composition, geometry, including lateral thickness variations and presence of possible

discontinuities, and age is just "educated guessing", based on various indirect premises and assumptions, and on regional geological context. This "guessing" could however be supported by various geophysical considerations that help to determine some of the aforementioned parameters.

Velocities and densities of igneous intrusions that are often higher than those of the host rocks (in particular in case of
35 sedimentary host rocks) result in sharp and significant changes of acoustic impedances related to such intrusions, and this in turn leads to high-amplitude seismic features observed on seismic reflection data (e.g. Hansen et al., 2004; Cartwright and Hansen, 2006; Hansen and Cartwright, 2006; Hansen et al., 2008; Miles and Cartwright, 2010; Magee and Jackson, 2020). Therefore, careful analysis of seismic data supported by seismic modelling might provide some semi-quantitative estimates of key petrophysical parameters characterizing studied deep igneous intrusions imaged by seismic reflection data. In this paper,
40 we present result of a study of regionally extensive system of deep high-amplitude seismic features imaged by regional high-end seismic data of the PolandSPAN® survey within the southwestern margin of the East European Craton in northern Poland. Main aim of this work was to constrain lithology, thickness and overall geometry of inferred igneous intrusions recognized at the depths of c. 6-7 – 19-20 km. Obtained results significantly improved understanding of the recently recognized Lublin Baltic Mississippian Igneous Province (Poprawa et al., 2024) and also deep igneous systems in general, including also geophysical
45 approaches towards determining their petrophysical characteristics.

2 Geological background

This study concerns inferred igneous intrusions detected imaged by deep seismic data within the crystalline basement of the Baltic Basin. This basin is located above the southwestern edge of the East European Craton (EEC), where the Precambrian crystalline basement is covered by Cambrian (locally also thin uppermost Ediacaran) to Silurian and Permian to Mesozoic and
50 Cenozoic sedimentary cover. The EEC extends from the Trans-European Suture Zone in central Europe to the Ural Mountains in the east - northeast (Fig. 1A). It is composed of three major crustal segments: Fennoscandia in the northwest, within which the study area is located, Sarmatia in the south, and Volgo-Uralia in the east (Fig. 1A; Gaál and Gorbatschev, 1987; Bogdanova et al., 1996). The EEC was formed during collisions and amalgamation around the Archaic nuclei, mainly during the 2.1–1.7 Ga time span (e.g. Gorbatschev and Bogdanova, 1993; Bogdanova et al., 2008; Johansson et al., 2022). The basement of the
55 Baltic Basin, similarly to the entire Fennoscandian domain, was consolidated during the late Svecofennian orogeny and associated metamorphism and igneous activity at approximately 1.87–1.75 Ga (Kheraskova et al., 2015; Krzemińska and Krzemiński, 2017; Krzemińska et al., 2021a).

In the Fennoscandian domain, the Svecofennian orogeny was followed by an intensive anorogenic igneous activity at approximately (1.67-) 1.54 to 1.45 Ga, resulting in the development of the anorthosite-mangerite-charnockite-granite (AMCG)
60 suite (Skridlaitė et al., 2003; Bogdanova et al., 2008; Krzemińska and Krzemiński, 2017). In the Sarmatian domain of the EEC, magmatism of a similar tectonic setting and chemical character took place earlier, at c. 1.81–1.74 Ga (Shumlyanskyy et al.,

2017). The presence of the AMCG-type intra-cratonic plutons is characteristic for the basement of the southern part of the Baltic Basin (Fig. 1A).
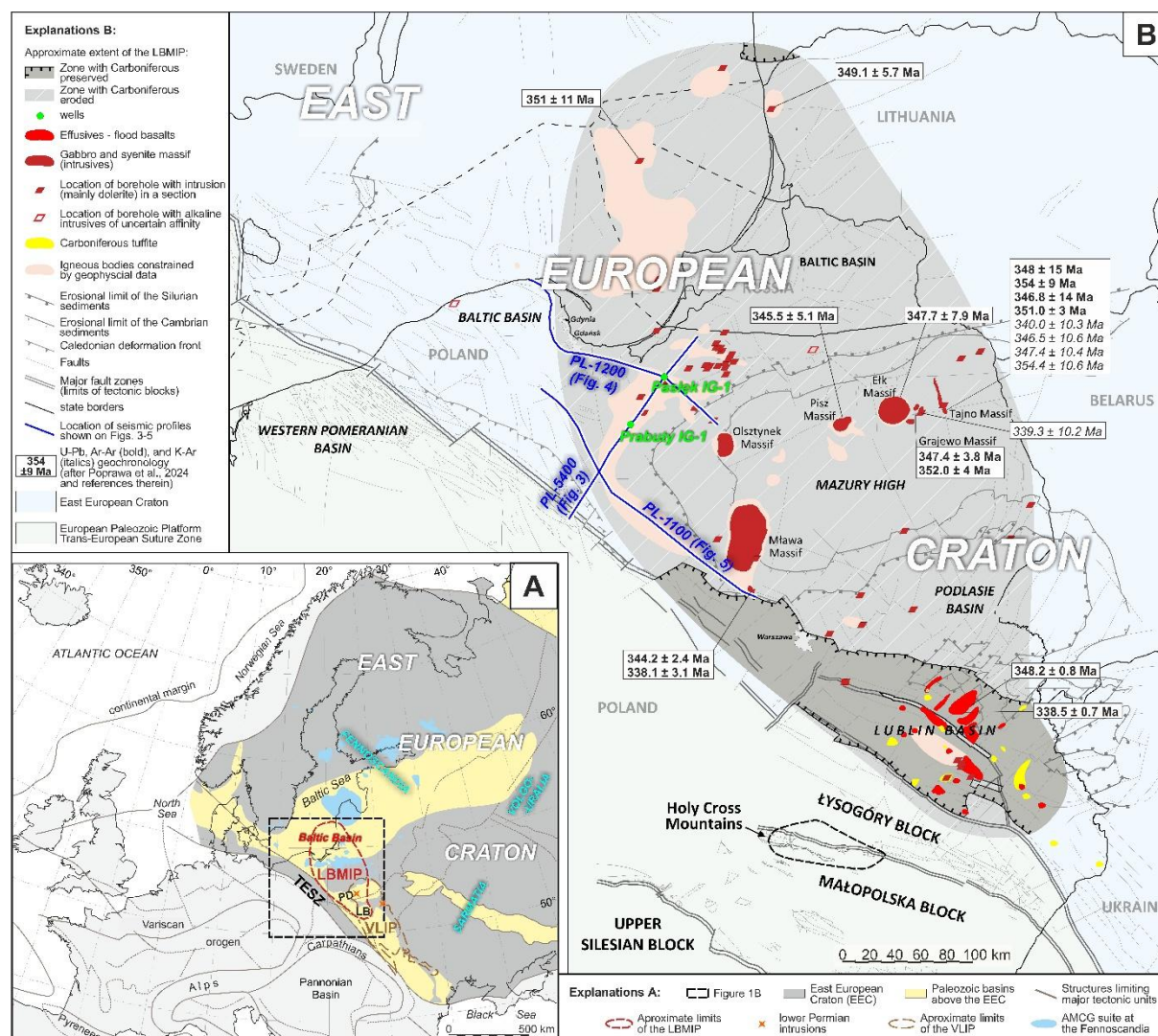
Figure 1: (A) The study area shown at the background of map of main tectonic units of Europe (after Berthelsen, 1992; Poprawa, 2020, supplemented). The lower Permian intrusions after Krzemińska et al. (2021b). LBMIP – Lublin-Baltic Mississippian Igneous Province, VLIP – Volhynia Large Igneous Province (upper Ediacaran; lateral extent after Kuzmenkova et al., 2010; Poprawa et al., 2020; Krzemińska et al., 2022), AMCG – anorthosite-mangerite-charnockite-granite suite (lateral extent after Andersson et al., 2001; Grabarczyk et al., 2023; Domańska-Siuda et al., 2024), PD: Podlasie Depression, LB: Lublin Basin, TESZ: Trans-European Suture Zone. **(B)** Regional map of NE Poland and surrounding areas that illustrates lateral extent of the Lublin-Baltic Mississippian Igneous Province (after Poprawa, 2019; Poprawa et al., 2024). Blue lines: location of PolandSPAN seismic profiles analysed in this paper (cf. Krzywiec et al., 2013, 2014).

75 The early Mesoproterozoic AMCG suite, together with the Svecofennian synorogenic granitoid and tonalite intrusions and supracrustal paragneisses, compose the crystalline basement of the study area. The basement is separated from the overlying upper Ediacaran–lower Paleozoic sedimentary cover of the Baltic Basin by an extensive stratigraphic gap that represents c. 900 My of denudation and hiatus. Development of the Baltic Basin, similarly to the sedimentary basins within other parts of the southwestern edge of the EEC, was initiated by the late Ediacaran rifting (Poprawa et al., 1999; 2018; Eriksson, 2012;

80 Krzywiec et al., 2018; Krzemińska et al., 2022). Southeast of the Baltic Basin, in the Podlasie, Lublin, and Volhynia-Podillya basins, rifting induced intensive magmatism and development of flood basalts and associated igneous and pyroclastic rocks of the Volhynia Large Igneous Province (VLIP) at c. (626-) 580-545 Ma (Fig. 1A; Shumlyanskyy et al., 2016; Poprawa et al., 2020; Krzemińska et al., 2022). However, the Baltic Basin was not affected by the late Ediacaran igneous activity, the northern limit of which was located approximately 200 km southeast of our study area (Fig. 1A).

85 Following the late Ediacaran rifting and the subsequent opening of the Tornquist Ocean, the western slope of the EEC became a passive continental margin of the newborn Baltica (Poprawa et al., 1999; 2018; Krzywiec et al., 2018). During that phase, succession of continental to shallow marine clastic Cambrian sediments was deposited within the Baltic Basin that passes up section into the Lower - Middle Ordovician clastics and carbonates (Areń and Lendzion, 1978; Modliński, 1982; Jaworowski, 1997).

90 During the Late Ordovician – Silurian times, Baltica's margin was under the influence of its oblique collision with Avalonia (e.g. Torsvik and Rehnström, 2003; Domeier, 2016). This resulted in development of the Caledonian fold-and-thrust belt and its foreland basin located along the western (present-day co-ordinates) slope of the EEC, including the Baltic Basin (Poprawa et al., 1999, 2018; Lazauskienė et al., 2002; Tari et al., 2012; Mazur et al., 2016, 2018). It was filled mainly with the fine-grained marine clastic sediments of significant thickness, locally exceeding 5000 m (Podhalańska and Modliński, 2006;

95 Krzywiec et al., 2013, 2014; Mazur et al., 2016; Porębski and Podhalańska, 2019; Poprawa, 2020). The development of the Baltic Basin continued during the Devonian and early Mississippian, when several hundred meters of mainly fluvial and deltaic clastic and marly sediments were deposited (Maryja, 2006). However, these sediments were removed by the Carboniferous and/or early Permian erosion, except for the easternmost part of the basin. The uplift that caused this pervasive denudation might have been at least partly driven by the regional far-field compressional stress transmitted into the foreland plate from

100 the Variscan collision zone (Krzywiec et al., 2017a, 2017b; see also Krzywiec et al., 2022).

  During the Mississippian, in the central and southern Baltic Basin, as well as in the adjacent Mazury High and Podlasie and Lublin basins located towards the southeast, intensive alkaline magmatic activity took place, considered to represent the distinct Lublin-Baltic Mississippian Igneous Province (see Fig. 1B; Poprawa, 2019; Poprawa et al., 2024). It has been best recognized within the Mazury High south of the Baltic Basin, where, due to uplift and denudation, the crystalline basement is

105 present at relatively small depth, commonly less than 1 km. In this area Mississippian alkaline igneous massifs were identified by numerous boreholes (e.g. Demaiffe et al., 2013; Krzemińska and Krzemiński, 2017; Wiszniewska et al., 2020; Fig. 2).
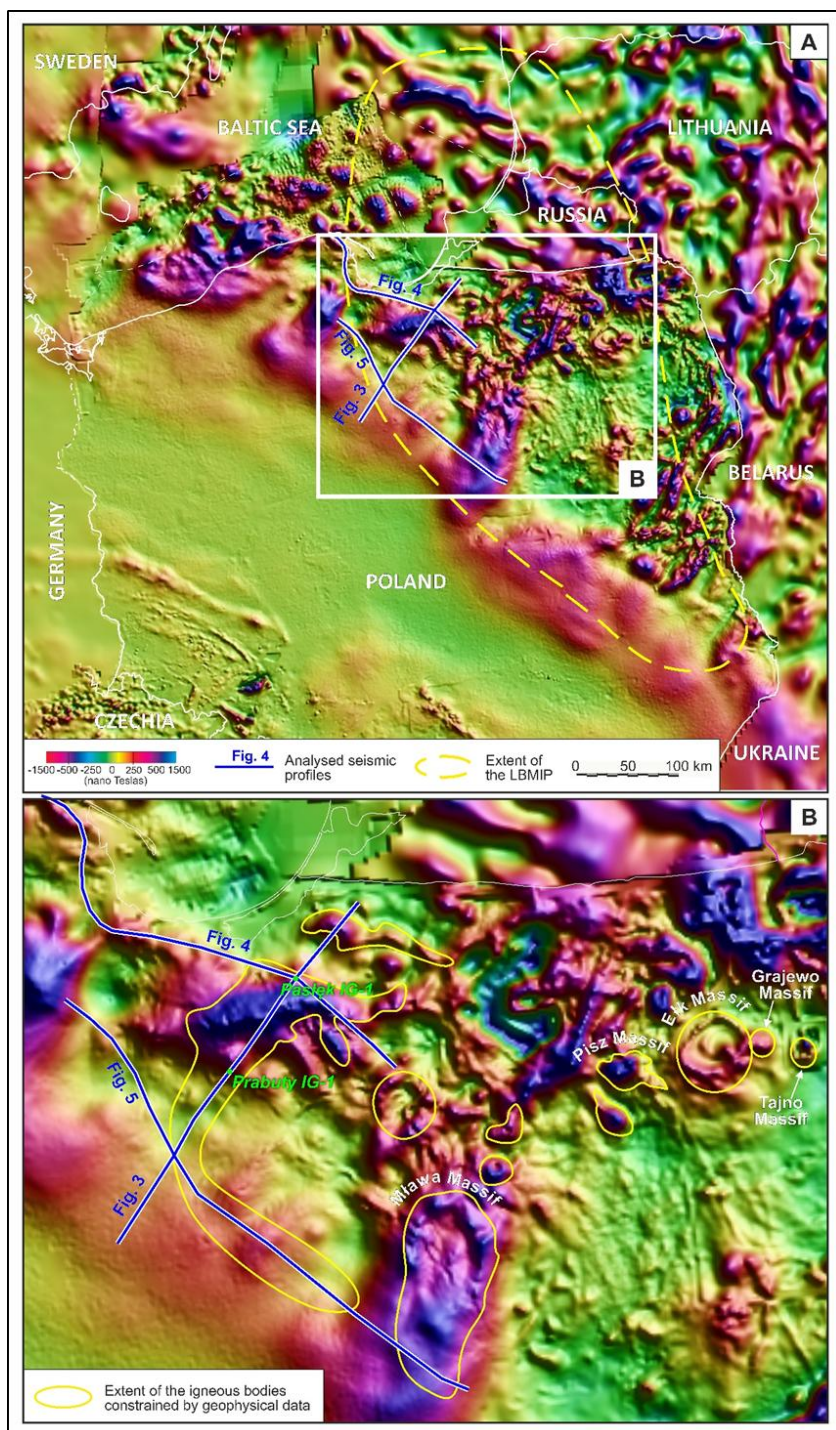
Figure 2: (A) Total intensity magnetic anomaly map of Poland (cf. Królikowski and Wybraniec, 1996; Wybraniec, 1999; Petecki and Rosowiecka, 2017). (B) Zoom into the study area with the igneous bodies constrained by geophysical data (after Poprawa et al., 2024, modified) and the location of igneous massifs identified by boreholes. Blue lines: location of PolandSPAN seismic profiles analysed in this paper (cf. Krzywiec et al., 2013, 2014).

The current geochronological data constrain period of development of these massifs at c. 352–344 Ma (Krzemińska et al.,
115   2025). Igneous intrusions, mainly dolerite sills, within the pre-Permian sedimentary cover of the EEC of the same age have
been recognized throughout the entire LBMIP (Fig. 1B; Poprawa et al., 2024). Effusive products of this igneous activity have
been largely eroded during the late Carboniferous and/or early Permian uplift, except for the southern part of the LBMIP, from
the study area, where the Mississippian basalts and tuffs have been preserved and encountered by numerous wells (Fig. 1B;
Pańczyk and Nawrocki, 2015; Poprawa, 2019).

120   During the latest Carboniferous to early Permian, vast parts of central and northwestern Europe, including the Western
Pomeranian Basin located to the west of the Baltic Basin, were covered with calk-alkaline effusives and pyroclastic rocks,
associated with intrusives (Neumann et al., 2004; Breitkreuz et al., 2007; Maliszewska et al., 2016). However, the EEC,
including the Baltic Basin, was devoid of that magmatic activity. The only exception is dolerite intrusion in the Podlasie Basin
(Krzemińska et al., 2021b), located however more than 200 km southeast from our study area.

125   Following extensive post-Variscan erosion, the study area was incorporated into the eastern flank of the Permian-Mesozoic
Polish Basin that belonged to the Central European Basin System (Dadlez and Marek, 1997 Maystrenko et al., 2008). This led
to the additional burial of the Baltic Basin Paleozoic sedimentary infill and its crystalline basement by c. 1.5-4 km, depending
on exact location. The upper Permian section is composed of the (Cisuralian – lower Lopingian) clastics and Zechstein (upper
Lopingian) evaporites and carbonates (Wagner, 1994; Kiersnowski, 1998; Peryt et al., 2010). The Triassic to the Lower
130   Cretaceous succession is dominated by clastic deposits (Dadlez and Marek, 1997), while the Upper Cretaceous, deposited
during basin inversion, consists of chalk and locally more coarse-grained syn-inversion deposits (see Stachowska and
Krzywiec, 2023 and references therein). Following Late Cretaceous – Paleogene inversion, uplift and erosion (Krzywiec, 2006;
Stachowska and Krzywiec, 2023), the Permian-Mesozoic succession was covered by a mostly flat-lying up to 200-300 hundred
meters on average thick Cenozoic continental clastic sediments (Piwocki and Kramarska, 2004).

3 Data and methods

3.1 Seismic data

This study was based on selected profiles from the PolandSPAN® regional seismic survey located above the southwestern
edge of the East European Craton in Poland (cf. Krzywiec et al., 2013, 2014). This survey consists of approximately 2200 km
of onshore seismic reflection profiles acquired with high-end parameters such as broadband sweep (2-150 Hz), 960-channel
140   symmetric spread, 12 km long offsets, long record lengths (12 s), tight station spacing (25 m) and high nominal fold (480). All
the data was processed up to PreSTM and PreSDM. Nominal record length was 12 seconds, but in the field uncorrelated data
down to 28 seconds were recorded. Such approach to data acquisition and processing resulted in unparalleled imaging of the
entire Phanerozoic sedimentary cover and crust, down to MOHO (Malinowski, 2016). So far, PolandSPAN® data has been
used in order to reinterpret the Teisseyre-Tornquist Zone (Mazur et al., 2015, 2016) and to decipher and interpret deep tectonic

145 features within the crystalline basement (Mężyk et al., 2019, 2021), shed a new light on Ediacaran rifting of the cratonic edge (Krzywiec et al., 2018), helped to better constrain deeply buried Caledonian (Mazur et al., 2016) and Variscan (Krzywiec et al., 2017a,b; Kufrasa et al., 2020) orogenic fronts, and to reinterpret regional tectonics and depositional evolution along the cratonic edge during the Late Cretaceous inversion of the Polish Basin (Stachowska and Krzywiec, 2023). Recently, PolandSPAN® profiles have been used to provide new insight on lower Carboniferous igneous intrusions within the Baltic

150 and the Lublin basins in northern and southeastern Poland, respectively (Krzywiec et al., 2024; Poprawa et al., 2024).

For this study, three profiles of the PolandSPAN® survey have been analysed: PL-5400 (Fig. 3), PL-1200 (Fig. 4) and part of PL-1100 (Fig. 5). They were calibrated using data from deep wells that drilled to the base of the Lower Paleozoic sedimentary cover or reached top of the crystalline basement (cf. Krzywiec et al., 2013, 2014; Mazur et al., 2016; Stachowska and Krzywiec, 2023).

155
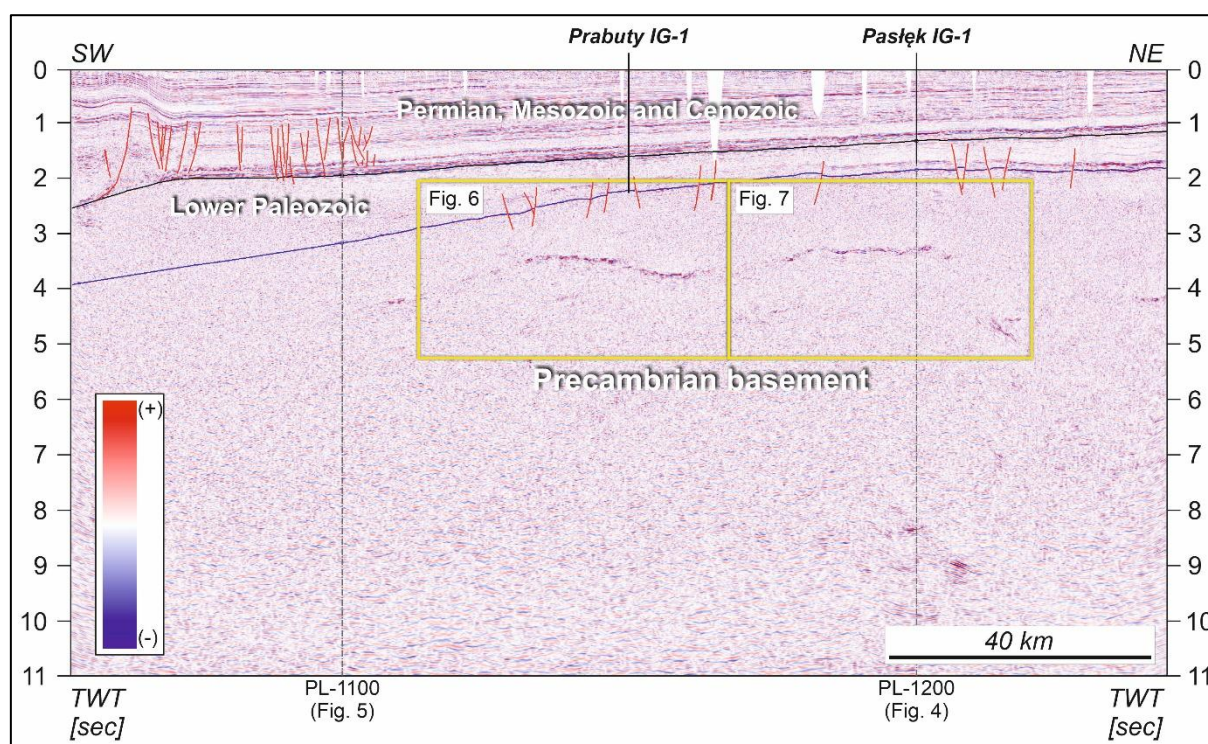
Figure 3: PolandSPAN seismic profile PL-5400 that imaged high-reflectivity zones – inferred igneous intrusions - within the crystalline basement described in this paper. Location see Fig. 1 and Fig. 2.
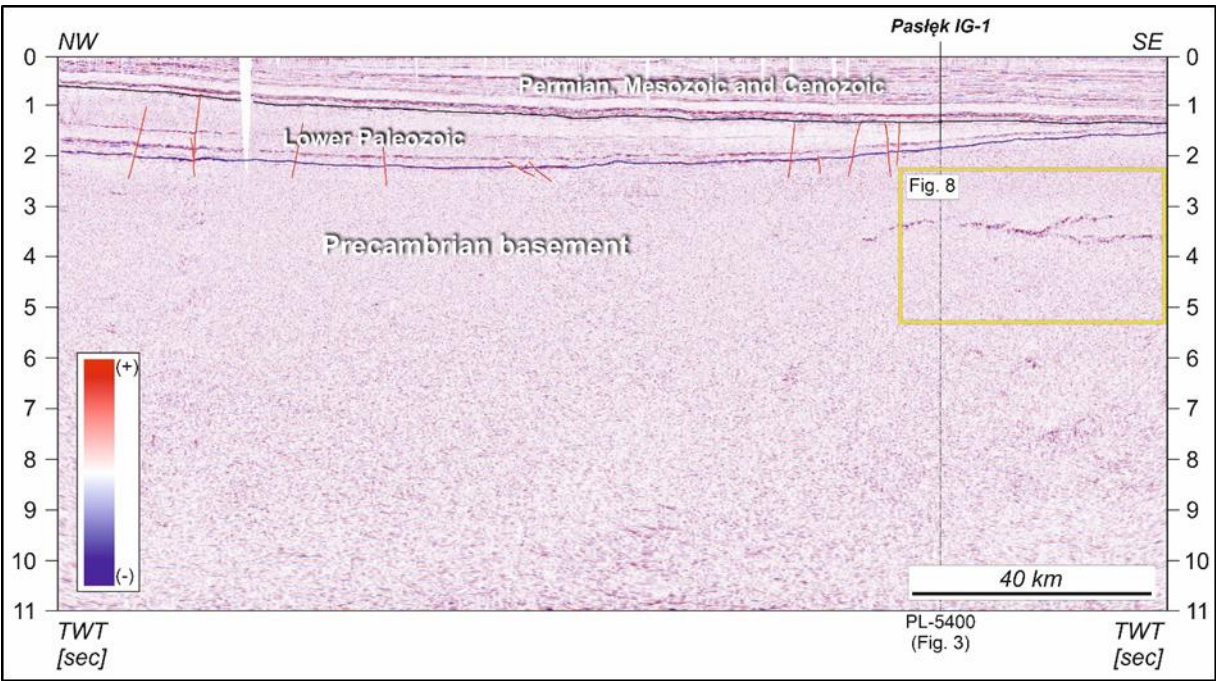
160 **Figure 4: PolandSPAN seismic profile PL-1200 that imaged high-reflectivity zones – inferred igneous intrusions - within the crystalline basement described in this paper. Location see Fig. 1 and Fig. 2.**
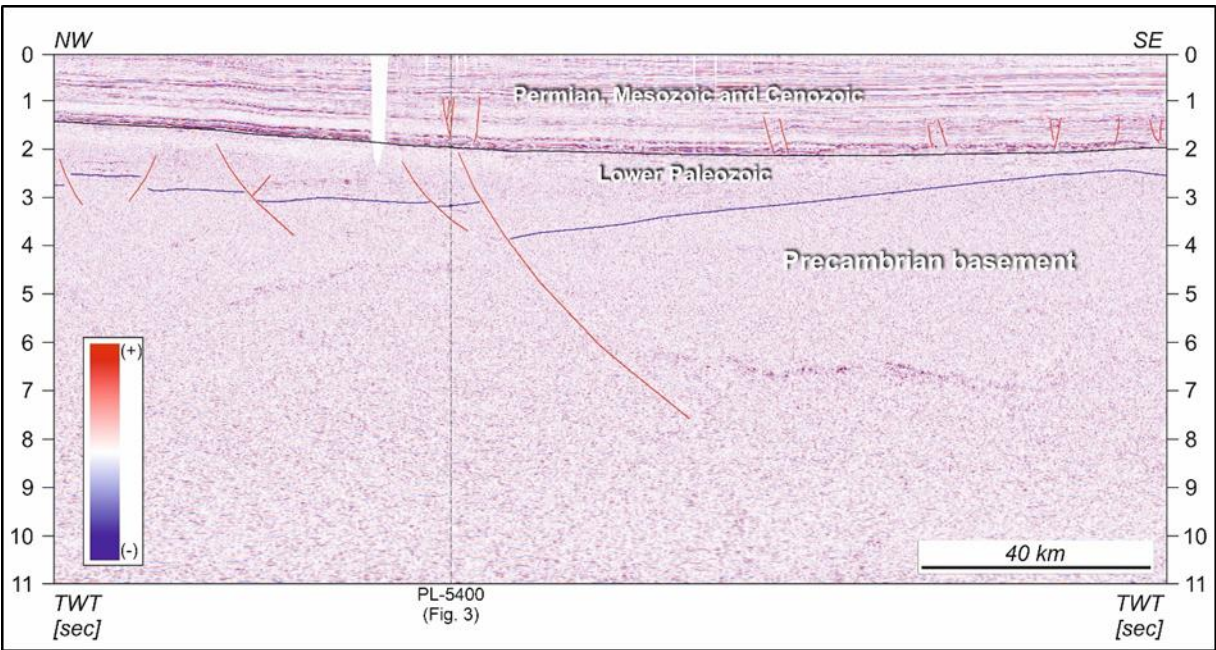
Figure 5: NW part of PolandSPAN seismic profile PL-1100 that imaged high-reflectivity zones – inferred igneous intrusions - within
165 **the crystalline basement described in this paper. Location see Fig. 1 and Fig. 2.**

3.2 Analysis of vertical seismic resolution

Quality of seismic imaging directly depends on seismic resolution, which is determined by the relationship between dominant frequency and interval velocity (e.g. Faleide et al., 2021). The final resolution of seismic data is also influenced by various processing algorithms, including those used for migration of seismic data (Sheriff, 2002; Cartwright and Huuse, 2005). Seismic resolution decreases with depth which is combined effect of two main factors: (i) general increase of velocity with depth due to mechanical and chemical compaction, and (ii) increased attenuated of higher frequencies with depth (Brown, 2011; Bjørlykke, 2015; Faleide et al., 2021).

The vertical seismic resolution, regarded as the limit of vertical separability of seismic events / features, is defined as quarter of a seismic wavelength used in a given seismic survey ($\lambda/4$; e.g. Brown, 2011), whereas precise limits of visibility or detectability can vary depending on the quality of the seismic data (Faleide et al., 2021; see also Brown, 2011, for more details). All of the above information was essential for conducting a detailed analysis of the vertical seismic resolution in areas where magmatic intrusions had been identified. The objective of analysis of vertical resolution was to determine the key parameters necessary for determining, or estimating, the thickness of igneous intrusions imaged within the basement of the Baltic Basin. Estimation of vertical seismic resolution was performed in two steps: (i) by advanced tuning analysis using wavelets extracted by a statistical method within the defined TWT windows, and (ii) by detailed analysis of the wedge model.

3.3 Seismic forward modelling

Seismic forward modelling was used to constrain, or to provide "educated guess" on the continuity, thickness, and lithology of inferred igneous intrusions identified on seismic data. The applied modelling methodology was based on a full-wave algorithm that generates multiple reflections. It provides a more accurate representation of wave propagation in a real medium than standard ray-tracing methods. The vertical incidence method was used to solve the wave equation by simulating the vertical propagation of P waves. This simple algorithm quickly evaluates the arrival time and amplitude of reflected waves, making it a very useful tool for seismic analysis. It is very effective methodology for studying the direct seismic response to lithology, and for verifying geological concepts when interpreting seismic data. The same approach has been recently tested and successfully used to study Upper Jurassic carbonate build-ups in southern Poland (Słonka et al., 2025).

For theoretical wave field calculations, we used zero-offset variant, which simulates synthetic stacked and migrated seismic profiles. Seismic modelling involves simulating seismic wave propagation in two-dimensional, geologically representative numerical models. Each modelling scenario begins with the creation of seismic-geological model in depth domain that consists of seismo-geological layers i.e. polygons with assigned P-wave velocities and densities (cf. Fagin, 1991; Rabbel et al., 2018; Lecomte et al., 2015; Li and Mitra, 2020a, b; Słonka et al., 2025). Following the construction of various seismic-geological models and definition of the acquisition parameters, simulations were performed using the specified theoretical wavelet.

3.3.1 Determination of lithology

One of the key steps in this study was estimation of possible lithological characteristics of inferred deep igneous intrusions as several viable options could have been considered. To achieve this, we constructed seismic-geological models based on seismic profile PL-5400 (Fig. 3). Geometry of each of these models, that included Phanerozoic sedimentary cover as well as upper

200 part of the basement together with inferred deep igneous intrusion, was derived from interpreted seismic profile. Each of the layer within the model was assigned specific velocities and densities.

Velocities for the sedimentary cover were based on data from two deep research wells Pasłęk IG-1 and Prabuty IG-1. For the basement, we assumed vertical velocity gradient. Its upper value was based on data from Prabuty IG-1 well that drilled topmost part of the basement, and its lower value was derived from deep seismic refraction studies (Grad et al., 2016).

205 Densities, due to lack of modern density logs, have been calculated using Gardner equation (Gardner et al., 1974). This approach was regarded as fully acceptable as our modelling study was focused on deep intra-basement seismic features, and generalized density distribution based on the Gardner equation was deemed as suitable for that purpose.

None of the studied high-amplitude seismic events visible within the basement of the Baltic Basin have been reached by wells so we relied on literature data on velocities and densities for three main lithologies that were tested during modelling study,

210 i.e. granite-granodiorite, basalt and dolerite (Dortman and Magid, 1969; Murase et al., 1973; Plewa and Plewa, 1992; Brown and Kim, 2020; cf. McBride et al., 2004).

Seismic modelling was performed using a theoretical 30 Hz Ricker signal that is close approximation of a wavelet extracted from the entire PL-5400 seismic profile using statistical method. Recording time for each simulation was set to eight seconds, and the trace/CMP interval was set to 20 meters as these parameters matched acquisition parameters of the PolandSPAN®

215 seismic data.

Calculated synthetic seismic profiles have been then compared to real seismic data, with particular focus on seismic imaging of deep igneous intrusions, on amplitude characteristics, and on continuity of particular seismic horizons. This comparison allowed to select the most probable lithological interpretation for deep seismic events visible on PolandSPAN® data within the basement of the Baltic Basin.

220 ### 3.3.2 Determination of seismic wavelet and vertical resolution - wedge model

We applied a theoretical seismic modelling approach based on wedge models in order to determine the exact seismic constraints related to the seismic wavelet and the vertical resolution of the analysed seismic dataset. Similar methodology has been applied in the past for other studies of igneous intrusions wavelet estimation and analysis of vertical seismic resolution (e.g., Hansen et al., 2008; Eide et al., 2017; Wrona et al., 2019; Köpping et. Al., 2022; Zeng et al., 2023; Cartwright et al.,

225 2025). In our study, analysing the wedge model was essential for determining the possible thickness and an overall geometry and lateral continuity of inferred deep igneous intrusions imaged on seismic data within the basement of the Baltic Basin.

The geophysical properties of the model layers were consistent with the densities and velocities assumed for inferred igneous intrusions that formed our wedge, and for the crystalline Precambrian basement that formed host rock for the wedge. The seismic response of the wedge model was calculated using a zero-phase 30Hz Ricker signal, deemed as reliable approximation
230 of an actual seismic wavelet used for the PolandSPAN® seismic survey. The resulting synthetic section was computed using the full-wave method (cf. Słonka et al., 2025).

4 Results

4.1 Analysis of vertical seismic resolution

We performed a detailed analysis of role of seismic tuning on analysed seismic data using statistical wavelets within the time
235 windows that covered igneous intrusions visible on seismic data. This analysis was crucial for subsequent steps, including seismic forward modelling and final estimation of vertical seismic resolution within specified data intervals where intrusions are visible. Ultimately, this has provided an approximation of the intrusion thickness. The analysis was carried out for seismic profiles PL-5400 and PL-1200 (Fig. 3 and Fig. 4), where high-reflectivity seismic events are located shallower (approximately 3,5-4,5 sec or 7-9 km, and 3-4 sec or 6,5-8,5 km, respectively) and are better visible than on profile PL-1100 (Fig. 5), where
240 analysed deep seismic features are located considerably deeper (approximately 6-7,5 sec or 16-19 km).
Seismic tuning refers to a phenomenon where the interference of waves from closely spaced reflections interfere and this might significantly affects apparent amplitude and apparent thickness of the resulting seismic reflector(s). This effect limits the vertical resolution of seismic data, which is important in so-called thin-bed analysis as reflections from top and base of a layer (bed) thinner than a quarter of the seismic wavelength (λ/4) cannot be reliably resolved as separate seismic horizons on
245 interpreted seismic data (Widess, 1973). For seismically thin beds (layers), seismic reflections from its top and base overlap and undergo interference, producing a single event of high amplitude. For geological layers characterized by thickness larger than λ/4, separate seismic reflections related to their tops and bases could be distinguished. The tuning thickness is the bed thickness for which two events related to top and base of the bed become indistinguishable on seismic data (e.g. Widess, 1973; Kallweit and Wood, 1982; Sheriff, 2002).
250 Detailed tuning analysis relies on tracking the tuning thickness based on the wavelet frequency content. To provide the necessary number of seismic trace samples for statistical analysis and to avoid distortion in the calculations, the wavelet extraction windows were set to 500 milliseconds. The three study polygons, two on profile PL5400 and one on profile PL-1200 have been examined in order to determine the maximum tuning thickness and the dominant frequency of each wavelet extracted within the specified time windows. The results have been then compared, and the average value of the calculated
255 dominant frequencies was used to determine the vertical seismic resolution in subsequent stages of our study.
Part of the PL-5400 seismic profile shown on Figure 6A reveals the south-western part of complex system of strong-amplitude reflections related to inferred igneous intrusion (cf. Fig. 3). The wavelet was extracted from all seismic traces within the specified time window (marked by the black dotted rectangle) using a conventional statistical method. To ensure full

comparability of the results, all analysed wavelets were 120 milliseconds long and sampled at 2 milliseconds. The calculated

260   amplitude spectra were characterized by relatively low noise content (Fig. 6B). Figure 6C presents the results of the tuning

analysis for the extracted wavelet, together with an estimation of the dominant frequency.

The tuning thickness chart (with all values in two-way travel time) consists of: (i) actual time thickness, which is the actual

bed thickness expressed in time units; (ii) apparent time thickness, which represents the isochron time between the top of the

layer (peak) and the base of the layer (trough), as measured from seismic data; (iii) a graph of the normalized peak-trough

265   amplitude that shows the peak amplitude of the combined peak/trough pair that encompasses the layer. In the final tuning

thickness charts, the blue curve is a cross plot of the apparent time thickness versus the actual time thickness. The apparent

time thickness (marked by black dotted curve) tracks the actual time thickness until it reaches a point known as the tuning

thickness. Below this point, however, it no longer tracks the actual time thickness; instead, it remains almost constant and

slightly smaller than the tuning thickness value. The red curve shows the cross plot of normalized peak-to-trough amplitude

270   against the actual time thickness. Starting at a value of 1 when the layer is relatively thick, it increases in amplitude as the bed

thins until the maximum amplitude is reached at tuning thickness. This maximum amplitude is produced by the constructive

interference of wavelets generated at the top and base of the studied layer. Below the tuning thickness, the curve decreases

almost linearly as the layer continues to thin.

The seismic tuning analysis of the first polygon (part of PL-5400 profile, Fig. 6) revealed a maximum normalized peak-to-

275   trough amplitude of approximately 1.4 at an actual time thickness of approximately 0.017 seconds. This indicates the tuning

thickness point, which is marked by the thin black horizontal line in Fig. 6C. The two-way time obtained through analysis was

multiplied by two to determine the period value (T). In this case, the multiplication yields a T value of 0.034 seconds. This

indicates that 29 Hz is the most likely dominant frequency within the examined time window of analysed part of PL-5400

profile, as illustrated on Fig. 6C.

280
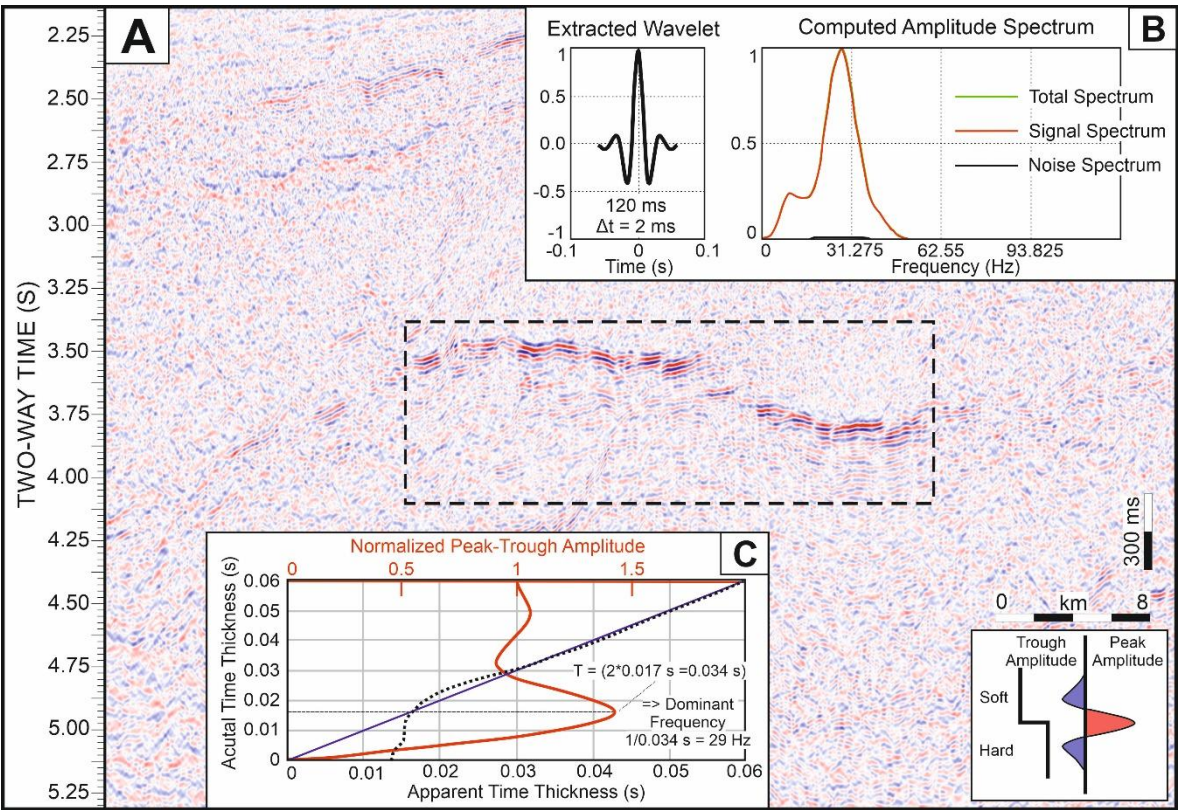
Figure 6: Seismic tuning analysis for polygon 1. (A) Enlarged part of PL-5400 seismic profile that illustrates detailed seismic expression of inferred igneous intrusion within the crystalline basement of the Baltic Basin (cf. Fig. 3). Black dotted rectangle indicates seismic wavelet extraction window for tuning analysis. (B) Extracted wavelet parameters with the computed amplitude
285 **spectrum. (C) Results of the seismic tuning analysis (tuning thickness chart) for the statistical wavelet extracted within a defined window, see text for additional explanation.**

The second polygon, also extracted from PL-5400 profile, illustrates northeastern part of the inferred igneous intrusion imaged by this profile (Fig. 7).

290
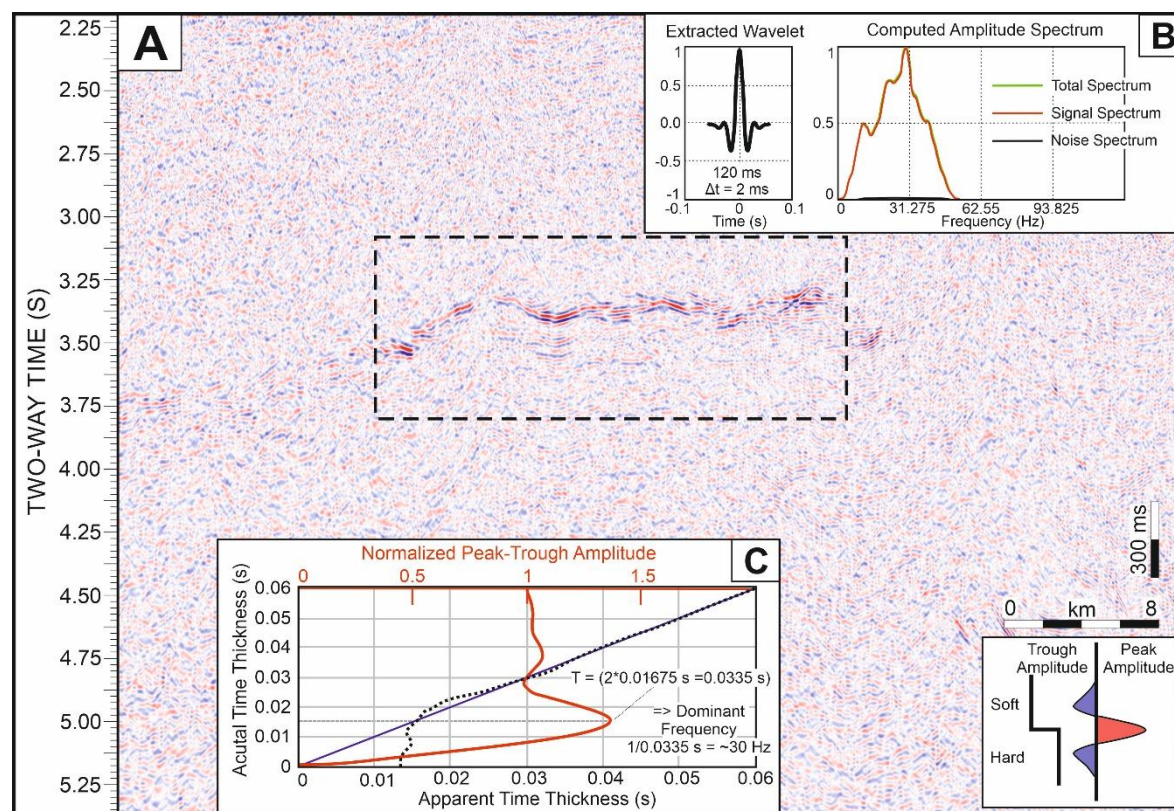
Figure 7: Seismic tuning analysis for polygon 2. (A) Enlarged part of PL-5400 seismic profile that illustrates detailed seismic expression of inferred igneous intrusion within the crystalline basement of the Baltic Basin (cf. Fig. 3). Black dotted rectangle indicates seismic wavelet extraction window for tuning analysis. (B) Extracted wavelet parameters with the computed amplitude spectrum. (C) Results of the seismic tuning analysis (tuning thickness chart) for the statistical wavelet extracted within a defined window, see text for additional explanation.

295

The time window used for wavelet extraction is marked by a black dotted rectangle (Fig. 7A). Calculated amplitude spectrum (Fig. 7B) is slightly broader than for polygon 1. This indicates a slightly augmented frequency content in this segment of the

300   PL-5400 profile in comparison to its southwestern counterpart. The tuning thickness chart (Fig. 7C) shows the results of the seismic tuning analysis that indicate that the maximum normalized peak-to-trough amplitude of approximately 1.3 was achieved at an actual time thickness of 0.0165 seconds. Thus, the calculated period value was approximately 0.0335 seconds. In this case, the dominant frequency within the examined time window of the second polygon is close to 30 Hz, slightly higher than in the first polygon.

305   The third polygon, based on part of the PL-1200 profile, imaged the most geometrically complex segment of the analysed inferred igneous intrusion (Fig. 8).
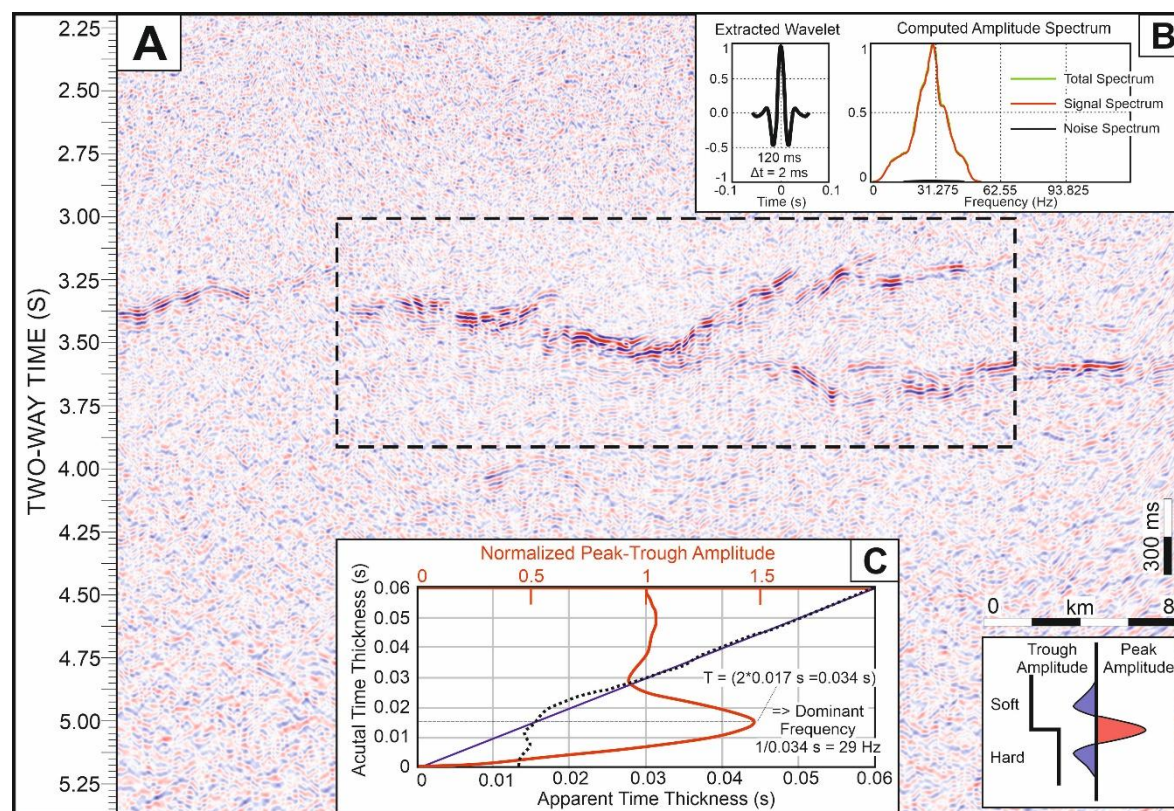
Figure 8: Seismic tuning analysis for polygon 3. (A) Enlarged part of PL-1200 seismic profile that illustrates detailed seismic expression of inferred igneous intrusion within the crystalline basement of the Baltic Basin (cf. Fig. 4). Black dotted rectangle indicates seismic wavelet extraction window for tuning analysis. (B) Extracted wavelet parameters with the computed amplitude spectrum. (C) Results of the seismic tuning analysis (tuning thickness chart) for the statistical wavelet extracted within a defined window, see text for additional explanation.

The wavelet extraction time window was more extensive than in previous polygons in order to capture all branches of strong reflectors associated to igneous intrusions, as shown by the black dotted rectangle on Figure 8A. The reflection amplitudes are comparable to those depicted on polygon 1 from profile PL-5400, resulting in concise amplitude spectrum (Fig. 8B). A seismic tuning analysis based on the tuning thickness chart (Fig. 8C) demonstrates a maximum normalized peak-to-trough amplitude of approximately 1.4 at an actual time thickness of approximately 0.017 seconds, which is the tuning thickness point. The period value was found to be 0.0034 seconds at that point, meaning that 29 Hz was the main frequency in the studied time window.

Based on an analysis of all the studied polygons, the average dominant frequency was found to be 29 Hz. Assuming velocity of approximately 6000–6700 m/s characteristic for igneous intrusion (see also below), the vertical seismic resolution according to the $\lambda/4$ criterion (Widess, 1973) would be approximately 52–58 meters. These results have then been used in the next stage of the vertical seismic resolution analysis based on wedge models.

4.2 Determination of lithology based on 2D seismic modelling

The aim of 2D seismic forward modelling was to study the seismic response of inferred deep igneous intrusions characterized by three alternative lithologies: granite-granodiorite, basalt and dolerite.

Velocities and densities of the model layers have been based on data from Pasłęk IG-1 and Prabuty IG-1 deep research wells

330 (Fig. 9). They are listed in Table 1.
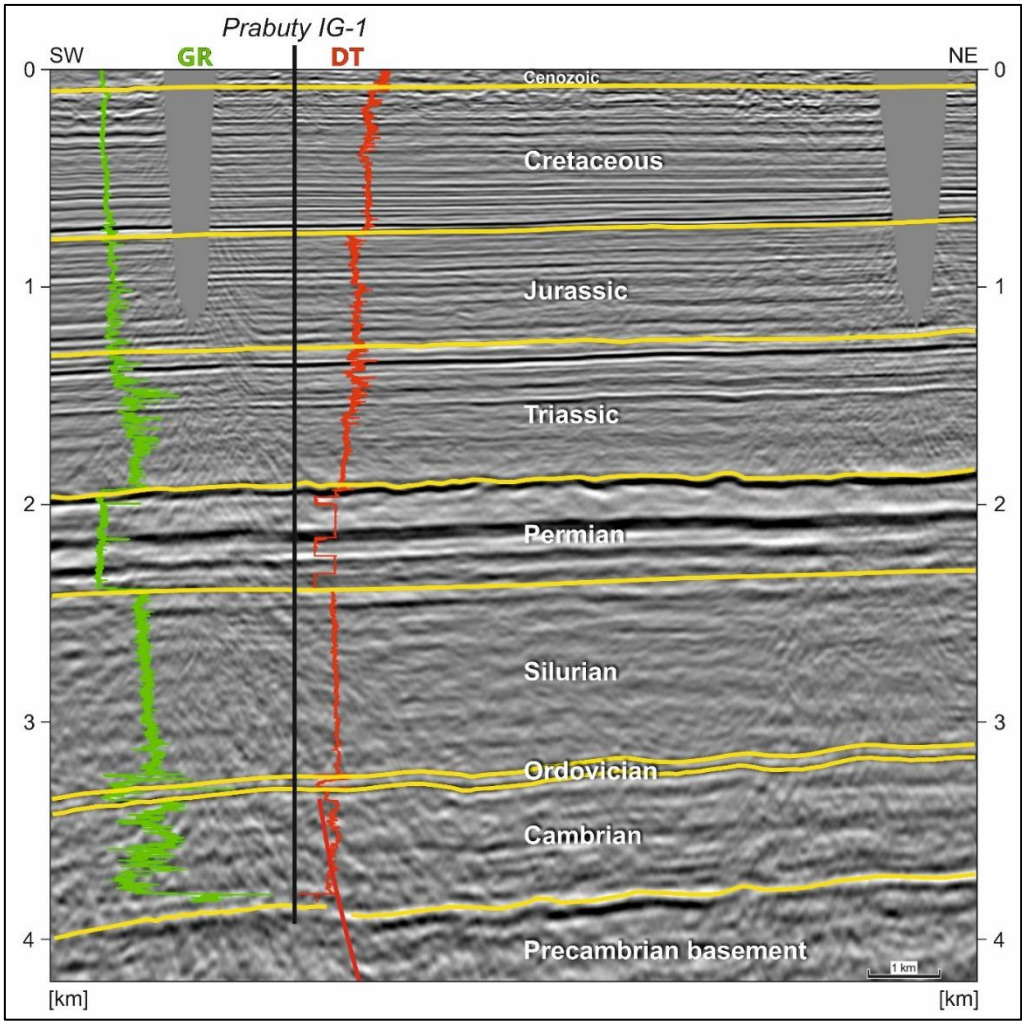
Figure 9: Correlation of deep calibration well Prabuty IG-1 with PSDM version of PL-5400 profile. GR: natural gamma ray log, DT: sonic log.

335 **Table 1. Velocities and densities for sedimentary cover and crystalline basement used for 2D seismic modelling.**

	stratigraphic interval	P-wave velocity (m/s)	density (g/cm^3)
1	Cretaceous and Cenozoic	2200	2.1

2	Jurassic	2500	2.2
3	Triassic	3200	2.23
4	Permian	5000	2.5
5	Silurian	4000	2.35
6	Ordovician	4300	2.4
7	Cambrian	4750	2.46
8	Precambrian basement	vertical gradient from 5500 to 6500	vertical gradient from 2.58 to 2.81

Two-dimensional seismic-geological model based on the PL-5400 seismic profile was 160 km long and 15 km deep. Three different lithological scenarios for igneous intrusions have been tested, for which petrophysical parameters have been derived from the literature:

340
1. granite-granodiorite: velocity = 5950 m/s; density = 2.67 g/cm³ (Dortman and Magid, 1969; Plewa and Plewa, 1992)
2. basalt: velocity = 6240 m/s; density = 2.76 g/cm³ (Murase and McBirney, 1973; Brown and Kim, 2020)
3. dolerite: velocity = 6700 m/s; density = 2.87 g/cm³ (Brown and Kim, 2020).

The results obtained for each modelling scenario are presented on Figures 10–12.

Conclusions regarding viability of each lithological scenario were based on comparison of modelled synthetic seismic data
345 with real seismic data. The qualitative assessment of the synthetic seismic data relied on observations of the reflection amplitude resulting from the contrasts in acoustic impedance between the intrusion and the host rock i.e. surrounding Precambrian crystalline basement. Fig. 10 illustrates modelling results for the granite-granodiorite scenario, characterized by minimum contrast of P-wave velocities and bulk densities between the intrusion and the host rock (Fig. 10A). Due to the very weak impedance contrast, the calculated synthetic seismic response from the modelled igneous body is characterized very low
350 amplitudes, much lower than on real seismic data (Fig. 10B). It should be stressed here that synthetic data is noise-free while real data contains seismic noise that can partly obscure the reflection amplitudes from the intrusion. Intrusion imaged by real seismic PSTM data (right panel on Fig. 10B), is, despite the noise, characterized by much higher amplitudes than synthetic data where intrusion is almost invisible (left panel on Fig. 10B). Observed difference in amplitude characteristics between modelled synthetic and real seismic data led us to the conclusion that granite – granodiorite lithology for the inferred igneous
355 intrusion should be deemed as very unrealistic.
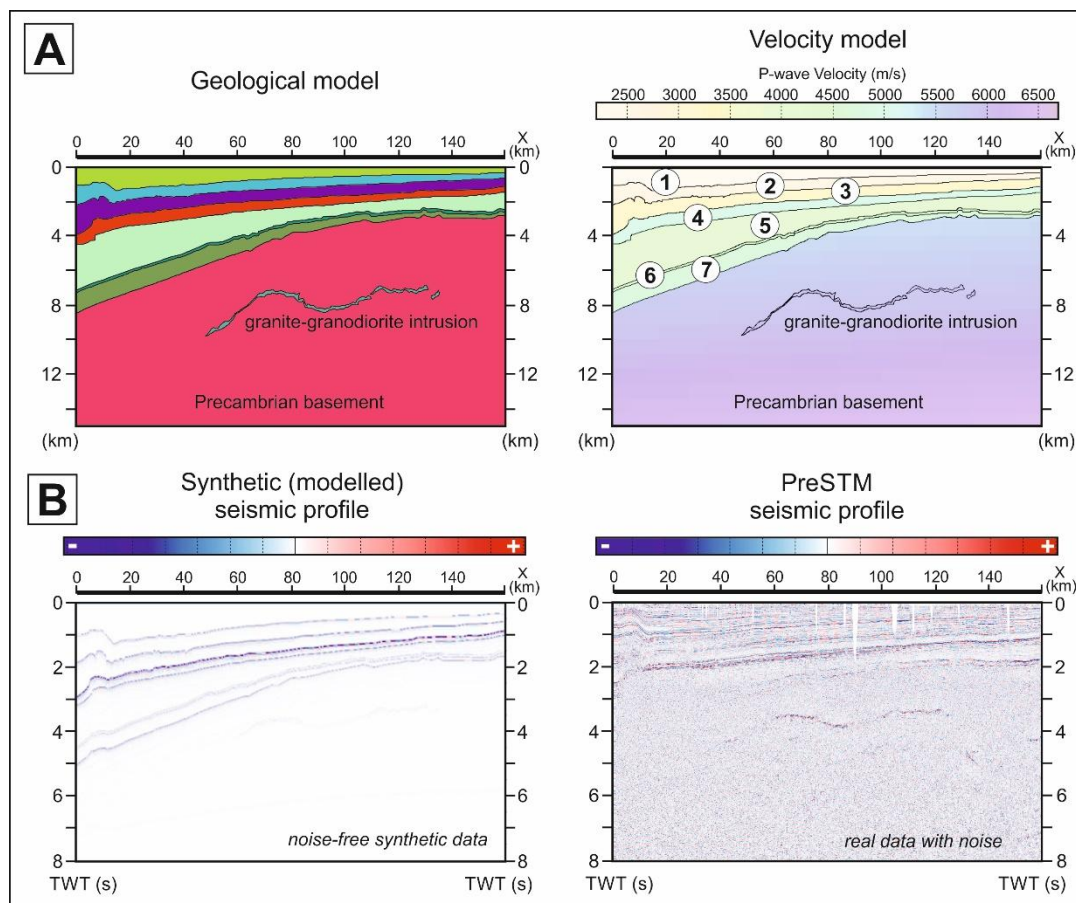
Figure 10: 2D seismic modelling for profile PL-5400 - granite-granodiorite scenario. (A) Left - geological model based on interpreted PL-5400 profile; right - P-wave velocity model: (1) Cretaceous and Cenozoic: velocity 2200 m/s, density 2.1 g/cm³, (2) Jurassic: velocity 2500 m/s, density 2.2 g/cm³, (3) Triassic: velocity 3200 m/s, density 2.23 g/cm³, (4) Permian (Zechstein evaporites): velocity 5000 m/s, density 2.5 g/cm³, (5) Silurian: velocity 4000 m/s, density 2.35 g/cm³, (6) Ordovician: velocity 4300 m/s, density 2.4 g/cm³, (7) Cambrian: velocity 4750 m/s, density 2.5 g/cm³, Precambrian basement: vertical velocity gradient 5500–6500 m/s, density gradient 2.58–2.81 g/cm³, granite-granodiorite intrusion: velocity 5950 m/s, and density 2.67 g/cm³ (after Dortman and Magid, 1969; Plewa and Plewa, 1992); (B) Comparison of synthetic profile and real PreSTM seismic profile.

360
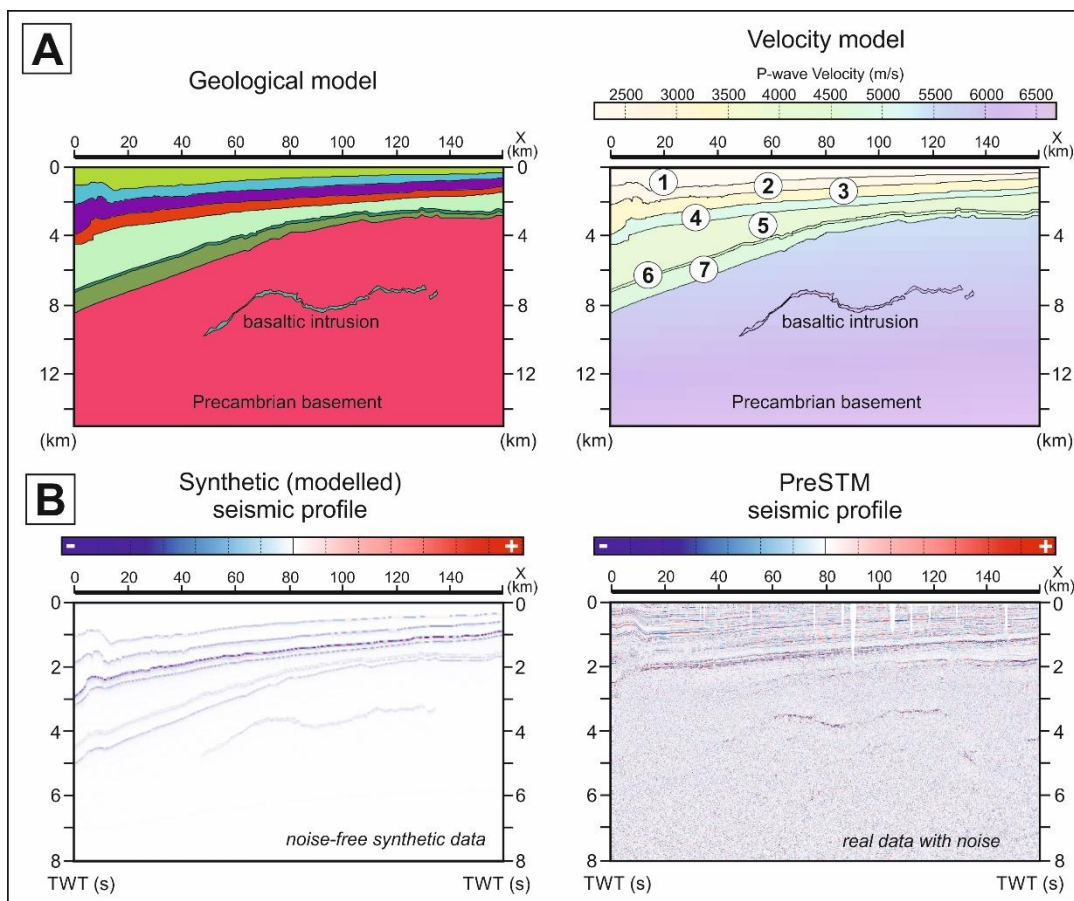
Figure 11: 2D seismic modeling for profile PL-5400 - basalt scenario. (A) Left - geological model based on interpreted PL-5400 profile; right - P-wave velocity model: (1) Cretaceous and Cenozoic: velocity 2200 m/s, density 2.1 g/cm³, (2) Jurassic: velocity 2500 m/s, density 2.2 g/cm³, (3) Triassic: velocity 3200 m/s, density 2.23 g/cm³, (4) Permian (Zechstein evaporites): velocity 5000 m/s, density 2.5 g/cm³, (5) Silurian: velocity 4000 m/s, density 2.35 g/cm³, (6) Ordovician: velocity 4300 m/s, density 2.4 g/cm³, (7) Cambrian: velocity 4750 m/s, density 2.5 g/cm³, Precambrian basement: vertical velocity gradient 5500–6500 m/s, density gradient 2.58–2.81 g/cm³, basaltic intrusion: velocity 6240 m/s and density 2.76 g/cm³ (after Murase and McBirney, 1973; Brown and Kim, 2020); (B) Comparison of synthetic profile and real PreSTM seismic profile.
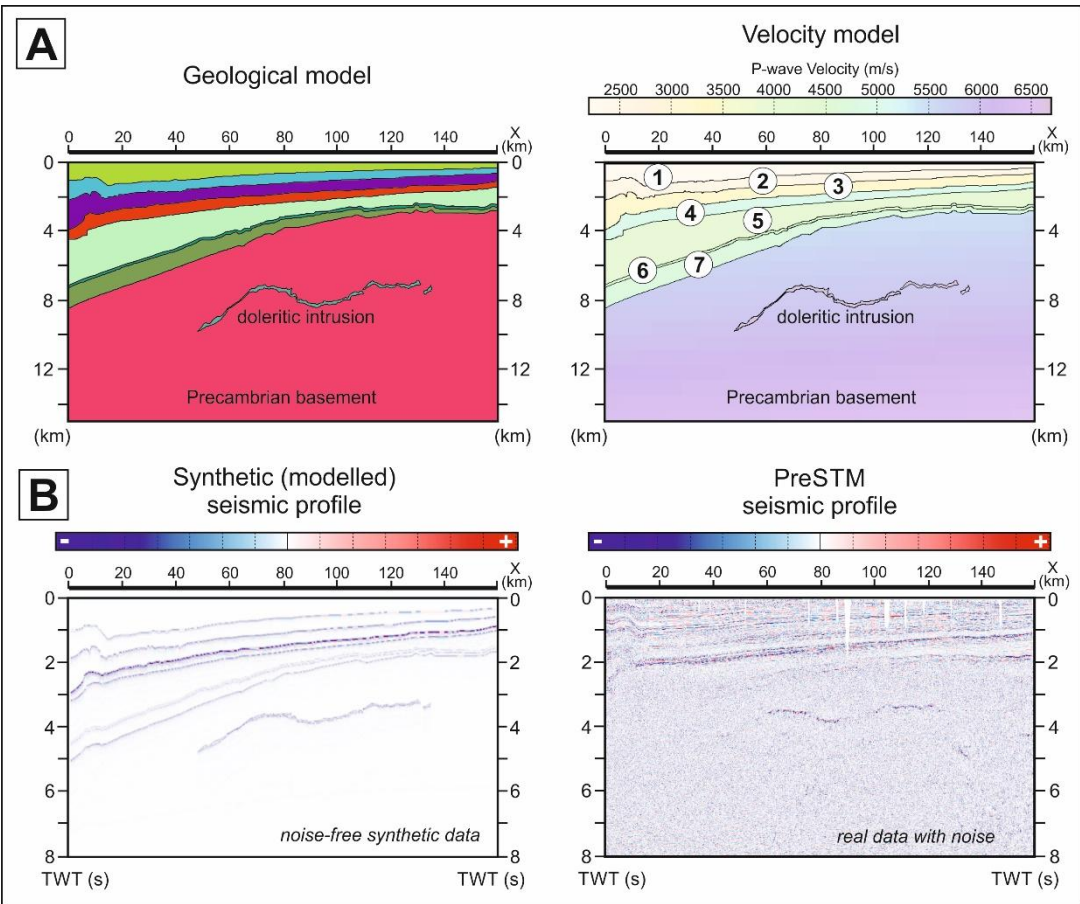
Figure 12: 2D seismic modeling for profile PL-5400 - dolerite scenario. (A) Left - geological model based on interpreted PL-5400 profile; right - P-wave velocity model: (1) Cretaceous and Cenozoic: velocity 2200 m/s, density 2.1 g/cm³, (2) Jurassic: velocity 2500 m/s, density 2.2 g/cm³, (3) Triassic: velocity 3200 m/s, density 2.23 g/cm³, (4) Permian (Zechstein evaporites): velocity 5000 m/s, density 2.5 g/cm³, (5) Silurian: velocity 4000 m/s, density 2.35 g/cm³, (6) Ordovician: velocity 4300 m/s, density 2.4 g/cm³, (7) Cambrian: velocity 4750 m/s, density 2.5 g/cm³, Precambrian basement: vertical velocity gradient 5500–6500 m/s, density gradient 2.58–2.81 g/cm³, doleritic intrusion: velocity 6700 m/s and density: 2.87 g/cm³ (Brown and Kim, 2020); (B) Comparison of synthetic profile and real PreSTM seismic profile.

The results of the seismic modelling used to assess the second lithological scenario of basaltic igneous intrusion are presented on Figure 11. In this case, we've been dealing also with relatively low P-wave velocity contrast between the intrusion and the host rocks of the Precambrian basement, and the contrast is even lower for bulk density (Table 1). As a result, due to comparable acoustic impedance of the intrusion and the host rock, the intrusion is characterized by a low amplitude seismic response (although not as low as in the former case of granite-granodiorite scenario), different from what could be observed on real seismic data (Fig. 11B). Taking this into account, basaltic lithology has also been deemed as not viable.

The third seismic modelling lithological scenario assumed petrophysical parameters typical for the doleritic intrusion (Brown and Kim, 2020). Figure 12 illustrates assessment of the dolerite scenario completed using the same methodology as described

390 before. In this case, significant contrast of P-wave velocities and significant difference in bulk densities exceeding 5% of the background values, resulted in a high-amplitude seismic image of modelled intrusion (left panel on Fig. 12B), comparable to amplitude characteristics of real seismic data (right panel on Fig. 12B). Taking this into account, and also the fact that numerous wells in the Baltic Basin, including Pasłęk IG-1 deep well located on profiles PL-5400 (Fig. 3) and PL-1200 (Fig. 4), have documented the lower Carboniferous dolerite intrusions, it was concluded that dolerite lithology is the most probable
395 approximation for the inferred igneous intrusion imaged by PolandSPAN® data within the basement of the Baltic Basin.

4.3 Wedge model

Apart from lithology, another important parameter that directly influences seismic imaging of inferred deep igneous intrusions visible on seismic data are lateral variations of their thicknesses. In order to estimate dominant thickness and its lateral variations, analyze the seismic tuning and vertical resolution a wedge model was used based on doleritic lithology to (Fig. 13).
400 The geophysical parameters of the wedge that simulates igneous intrusion were consistent with the P-wave velocity and bulk density used for 2D seismic modelling described above and equaled 6700 m/s and 2.87 g/cm^3, respectively (Fig. 12). The total length of the wedge is 1000 m, and its thickness changes from 0 to 200 m. The wedge model simulates zero-phase seismic data, and the resulting synthetic profile, shown in Fig. 13B, was computed using the full-wave modeling algorithm and 29 Hz Ricker dominant wavelet. Fig. 13C shows a graph that includes: (i) predicted normalized amplitude and (ii) apparent and actual
405 wedge thicknesses, based on Dowdell's (2020) numerical algorithm. We estimated critical values, such as the onset of tuning thickness ($\lambda/2$) and tuning thickness ($\lambda/4$), in accordance with Widess's (1973) criteria, where λ is the dominant wavelength (Fig. 13C).
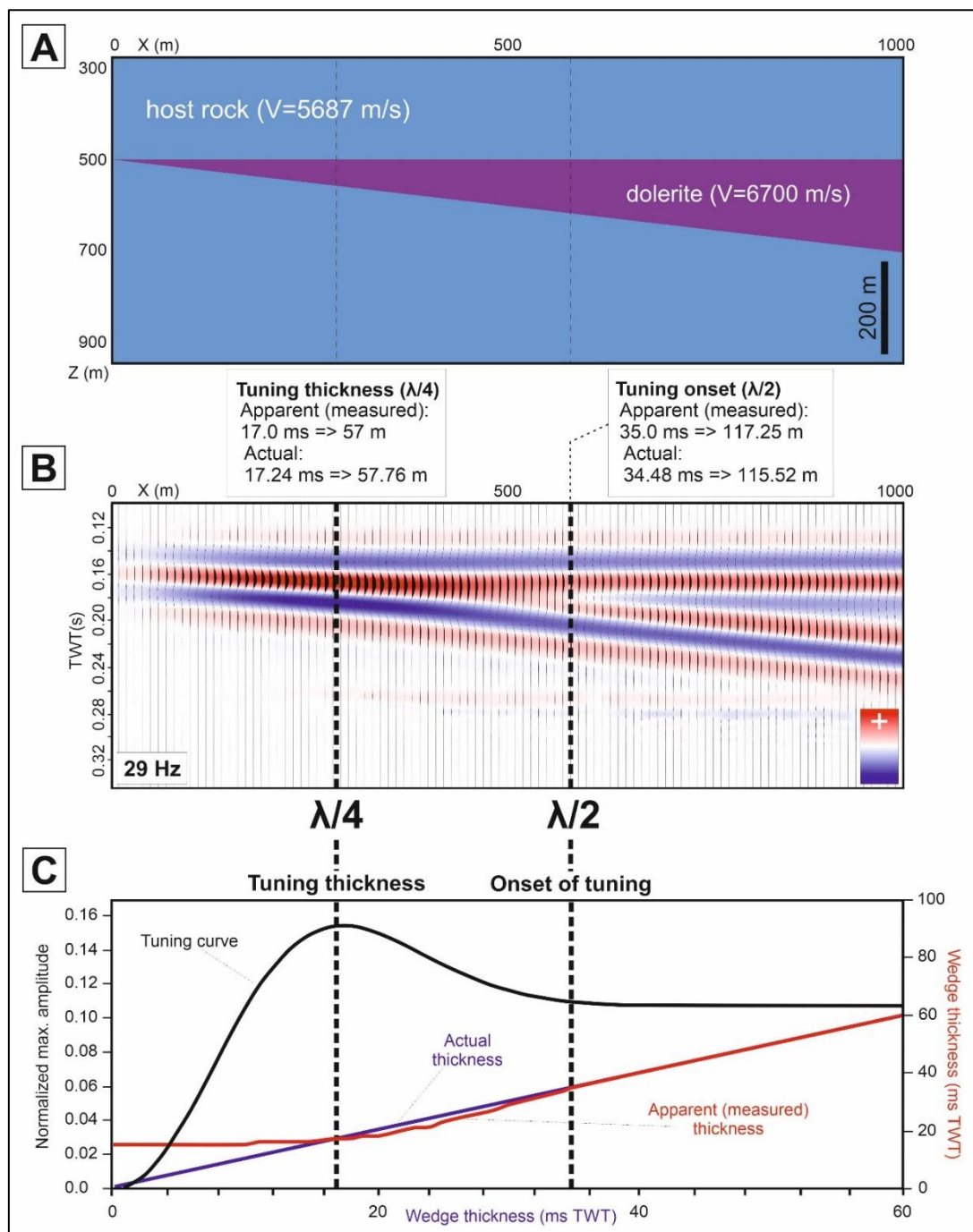
Figure 13: Wedge model used to evaluate role of tuning and vertical resolution of seismic imaging of dolerite intrusion. (A) wedge thickness ranges from 0 to 200 m, and the total length of the model is 1000 m, velocity and density values of the host rock have been 5687 m/s and 2.73 g/cm³, respectively, and for dolerite wedge 6700 m/s and 2.87 g/cm³, respectively (cf. Fig. 12). (B) Theoretical seismic profile obtained by using a zero-phase Ricker wavelet of 29 Hz (cf. Fig. 6, Fig. 7 and Fig. 8). (C) Graph of the tuning curve versus apparent and actual wedge thickness. Predicted amplitude displays maximum response at an estimated thickness of 57-58 m.

415

For intrusion 200 m to 115 m thick, the reflections from the top and base of the wedge could be easily separated (Fig. 13B). As the wedge thins to λ/2 thickness, the tuning curve begins to turn upward as reflections from the top and base start to interfere. Further thinning of the wedge results in increased constructive interference until it is thinned to a thickness of λ/4 (the tuning thickness), at which point the interference reaches its maximum (Fig. 13C). Peak of the tuning curve's indicates the minimum

420 thickness of the intrusion that can be resolved seismically which is approximately 57-58 meters (Fig. 13B). Below the tuning thickness (λ/4), destructive interference between the top and base wedge reflections prevail, and this leads to a substantial decrease in amplitude (Fig. 13C). Consequently, the top and base reflections from the intrusion become indistinguishable, precluding more detailed thickness estimation of the igneous body from seismic data.

4.4 Seismic interpretation of inferred deep igneous intrusions

425 Final step in this study was detailed interpretation of inferred igneous intrusions imaged by PolandSPAN® data that used as a reference point results of seismic modelling studies described in previous chapters. It involved three main steps: (i) detailed analysis of the reflection amplitude on the pre-stack time migrated (PreSTM) seismic data, (ii) assessment of the intrusion thickness based on seismic tuning and the vertical resolution criteria provided by the wedge model analysis, (iii) interpretation of intrusion top and base and analysis of its overall geometry.

430 Analyzed igneous intrusion are characterized by high amplitude seismic reflectors clearly visible within the Precambrian crystalline basement, which is typical for igneous intrusions imaged by seismic data (cf. Infante-Paez and Marfurt, 2018). The observed seismic reflections indicate that the analyzed intrusion is characterized by the following features: (i) partly lobate morphology, (ii) multiple, step-wise arrangements, and (iii) lateral thickness changes. This resembles lower crustal reflector system in the northern North Sea (Wrona et al., 2019), and seismic images of igneous intrusions from the North Sea basin

435 (Hansen and Cartwright, 2006), from the offshore Norway (Cartwright and Hansen, 2006), and from the eastern Scandinavian Caledonides (Juhlin et al., 2016).

As shown in Figures 14–16, the top of the intrusion is related to a positive amplitude reflection (peak), which is indicative of an increase in acoustic impedance. The top reflection demonstrates a moderate- to high-amplitude response, accompanied by periodic segments of amplification and dimming on variable length scales along the intrusion. These segments are indicative

440 of lateral amplitude variations associated with thickness changes. Amplitude response of intrusion top attains its maximum value at the tuning thickness. This peak is estimated when the intrusion thickness reaches approximately 58 m, in accordance with the λ/4 criteria established by Widess, 1973. As a result, reduced amplitude reflectors are expected when intrusion is thinner or thicker than this value.
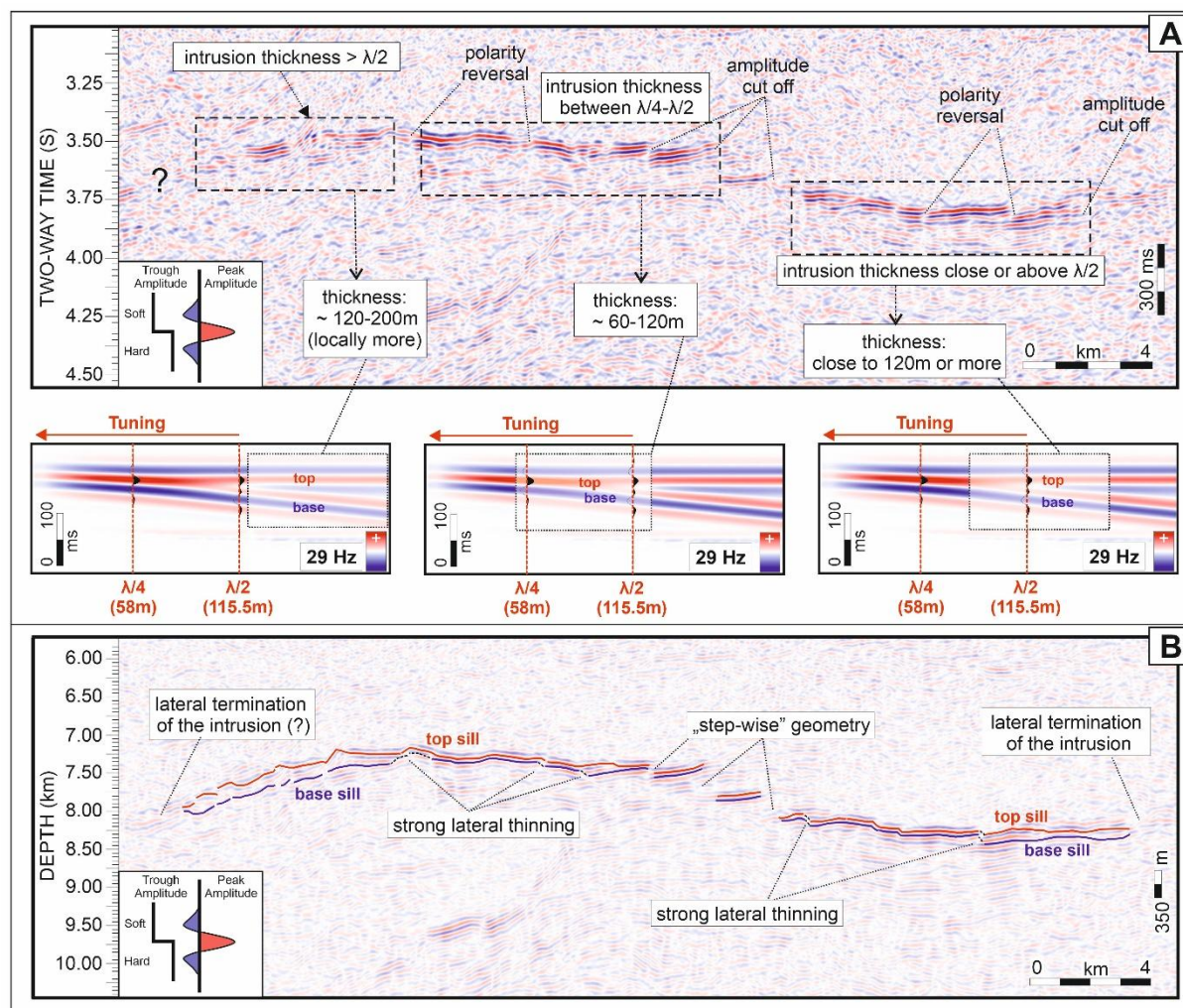
Figure 14: Seismic interpretation of igneous intrusion imaged by profile PL-5400, part 1 (cf. Fig. 6). (A) PreSTM seismic profile with detailed interpretation of reflection amplitude and an estimation of intrusion thickness based on seismic tuning and vertical resolution criteria obtained from the wedge model analysis (Fig. 13). Three wedge models, calculated using zero-phase Ricker wavelet with 29 Hz dominant frequency, demonstrate various seismic responses depending on different sill thicknesses; (B) Part of PreSDM PL-5400 profile that illustrates interpreted top and base of the intrusion and its inferred geometry.

The seismic image of the intrusion displays a close-to-tuned response over a substantial portion of the intrusion length (Fig. 14). The base of the intrusion is associated with negative amplitude, usually amplified but in some cases also dimmed, similarly to what could be observed for the top intrusion reflector. In areas where the inclination of the intrusion could be neglected, its base is often amplified, forming a specific amplified pair with the top reflector. Within the most of the analyzed area, it is possible to distinguish top and base of the intrusion, usually with some internal reflectivity between them. This suggests that the thickness of the intrusion is usually higher than the tuning thickness ($\lambda/4$). A reduction in reflection amplitude is often

observed in regions where intrusion are thicker, so the amplitude changes as the distance between the top and base reflections increases (Fig. 14A).

460 The lateral margins of the intrusion can be identified by an abrupt cut-off of seismic amplitudes. In certain regions, an abrupt decrease of reflection amplitude may be indicative of intrusion lateral termination. In other cases, the zone of reduced amplitude corresponds to its tapering thickness. However, the precise position of the tip cannot be determined more accurately because its exact shape cannot be resolved seismically (cf. Cartwright et al., 2025). Another salient feature of the intrusion's seismic image is diminishing of amplitude accompanied by a polarity reversal (Fig. 14A). This is frequently observed in
465 regions exhibiting substantial lateral variations in intrusion thickness, as illustrated in Figure 14B. Recently, Cartwright et al. (2025) described similar seismic features characteristics for the Dogger Sill Complex in the Southern North Sea.

Figure 14 presents results of interpretation of the southwestern part of the intrusion imaged by the PL-5400 profile. The intrusion thickness estimation was based on the analysis of the time seismic section (PreSTM; Fig. 14A) and it was verified by quantitative observations based on the wedge model (Fig. 13). Because the amplitude response is directly related to intrusion
470 thickness, the reflection amplitudes from the top and base of the intrusion could be analyzed using seismic tuning parameters and thickness values obtained from wedge model simulations. We then compared these results to the depth seismic section (PreSDM) and interpreted the top and base intrusion (Fig. 14B).

As shown in Figure 14A, the amplitude response indicates that interpreted intrusion thickness typically exceeds the maximum tuning amplitude ($\lambda/4$) and frequently approaches or surpasses the tuning onset ($\lambda/2$). The majority of amplified amplitudes are
475 observed in the central part of the intrusion. This suggests that the intrusion thickness is significantly reduced in this area. According to the wedge model, the thickness ranges from 60 to 120 meters, which corresponds to wavelength values between $\lambda/4$ and $\lambda/2$. In other segments, thickness of the intrusion is relatively larger, as evidenced by the partially separated reflectors from top and base of the intrusion. Reflection amplitude is only partially amplified, and internal (interfered) reflections are observed between the top and base horizons (the red and blue horizon picks in Fig. 14B). In these areas, the estimated intrusion
480 thickness generally exceeds 120 meters, locally exhibiting thicknesses of up to 200 meters or even more (Fig. 14B).

The seismic image of the entire intrusion is complex, with several amplitude cut-offs that are indicative of its lateral termination or tapering. Additionally, polarity reversals, another indicator of thickness changes, are clearly visible, highlighting areas of significant lateral thinning or thickening of the intrusion (Fig. 14A and Fig. 14B). The amplitude cut-off observed in the central part of the seismic profile in Fig. 14 indicates the presence of potential steps in the intrusion geometry, which likely manifest
485 as abruptly diminished amplitude and sharply reduced thickness. These irregular seismic reflections resemble the characteristic "step-wise" geometry (cf. Kavanagh and Sparks, 2011; Muirhead et al., 2012; Burgess et al., 2017). However, due to the large depth ranges and the lack of well control, the origin of the observed geometries remains unclear and requires further study using various intrusion analogues.
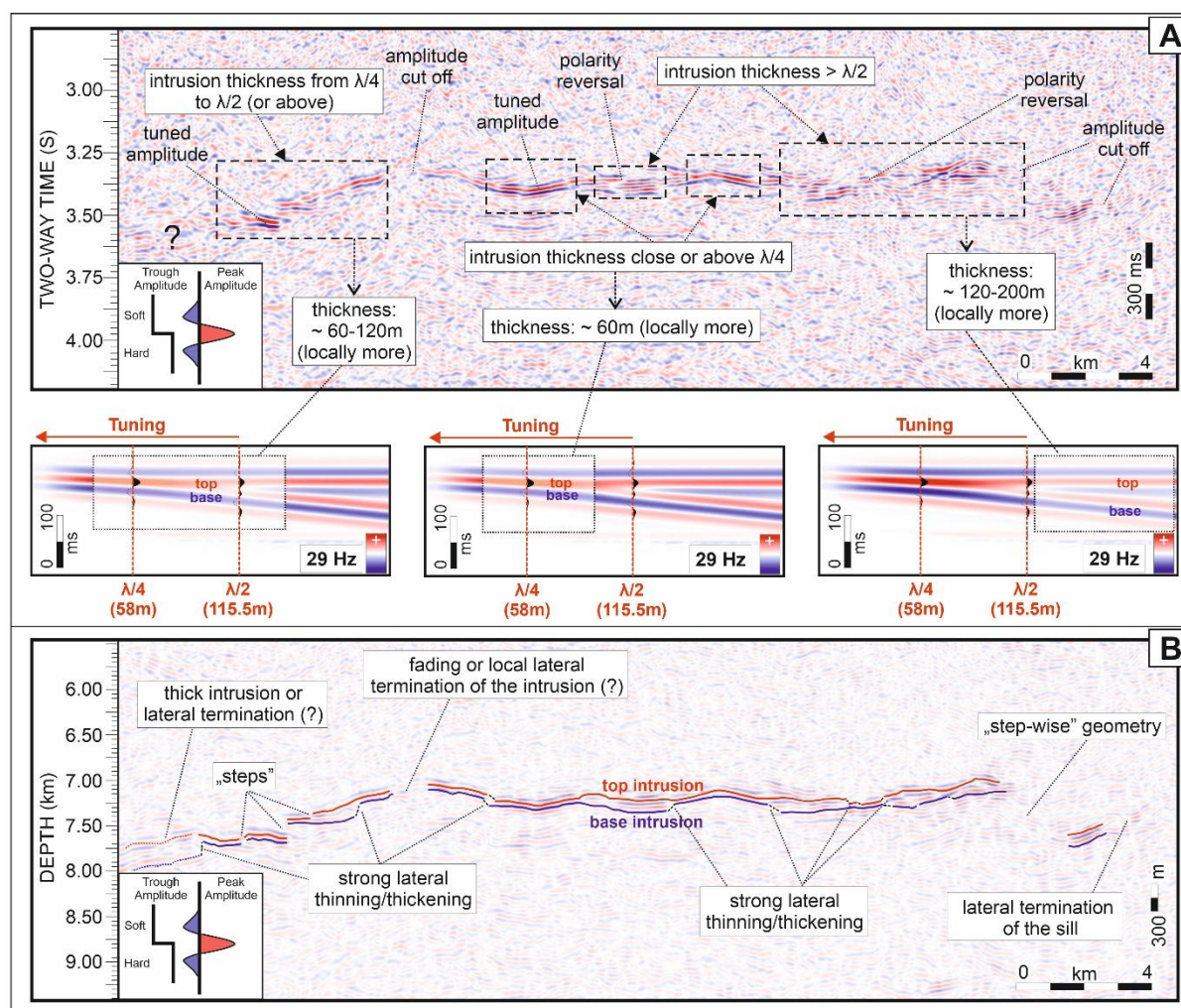
Figure 15: Seismic interpretation of igneous intrusion imaged by profile PL-5400, part 2 (cf. Fig. 7). (A) PreSTM seismic profile with detailed interpretation of reflection amplitude and an estimation of intrusion thickness based on seismic tuning and vertical resolution criteria obtained from the wedge model analysis (Fig. 13). Three wedge models, calculated using zero-phase Ricker wavelet with 29 Hz dominant frequency, demonstrate various seismic responses depending on different sill thicknesses; (B) Part of PreSDM PL-5400 profile that illustrates interpreted top and base of the intrusion and its inferred geometry.

A detailed interpretation of the northeastern part of the intrusion imaged by profile PL-5400 is presented in Figure 15. It reveals that intrusion lateral thickness variations are significantly more pronounced than those depicted in Figure 14. In many areas, the top and base of the intrusion can be clearly separated, with no evidence of amplitude amplification resulting from the seismic tuning effect which means that thickness exceeds the tuning onset ($\lambda/2$). In these cases, the estimated thickness of the intrusion significantly exceeds 120 meters, reaching up to 200 meters (Fig 15A).

A polarity reversal indicates significant lateral thinning or thickening. Tapering of the intrusion, local lateral terminations, and gradual amplitude fading are clearly visible as an amplitude cut-offs in the seismic image. A significant portion of the intrusion displays amplified or dimmed reflection amplitude, indicating that its thickness may fall within the range of λ/4 to λ/2, and is considerably influenced by tuning (Fig. 15A). In certain areas, the intrusion thickness approaches or slightly exceeds the maximum tuning thickness value (λ/4), as evidenced by the strongly tuned amplitudes. In these segments, the intrusion thickness can be reduced to approximately 60 meters (see Figs. 15A and Fig. 15B). On the other hand, the interpretation of the intrusions is locally unclear because instead of the expected amplitude cut-off associated with intrusion tapering, at some points it appears to represent clearly separated top and base intrusion reflections with medium amplitudes. This suggests the existence of an even intrusion body of higher thickness exceeding 200 meters. Classic "step-wise" geometries are also visible in the seismic data (Fig. 15B).

Profile PL-1200 imaged most complex part of the studied igneous intrusion (Fig. 16). The thickness of the intrusion varies considerably laterally, with multiple polarity reversal points and discernible amplitude cut-offs associated with its tapering or lateral termination (Fig. 16A). Dimming or local amplitude amplification, particularly when approaching a value of λ/4, is indicative of significant variations in sill thickness. In some areas, the sill thickness varies between 60 m and 120 meters.

The top sill reflection is influenced by seismic tuning in broader areas, as indicated by the wedge model, where the sill thickness aligns with the λ/4 - λ/2 criteria (Fig. 16A). On the other hand, a significant portion of the intrusion exhibits a reflection amplitude that far exceeds the tuning onset (λ/2), with thicknesses ranging from 120 to over 200 meters (Fig. 16B). This is especially evident in the central part of the sill. Intrusion features here multiple internal "steps" and small branches from the main intrusive body. The interpretation of some of these features remains ambiguous, although the main sill branching could be clearly observed (Fig. 16B).
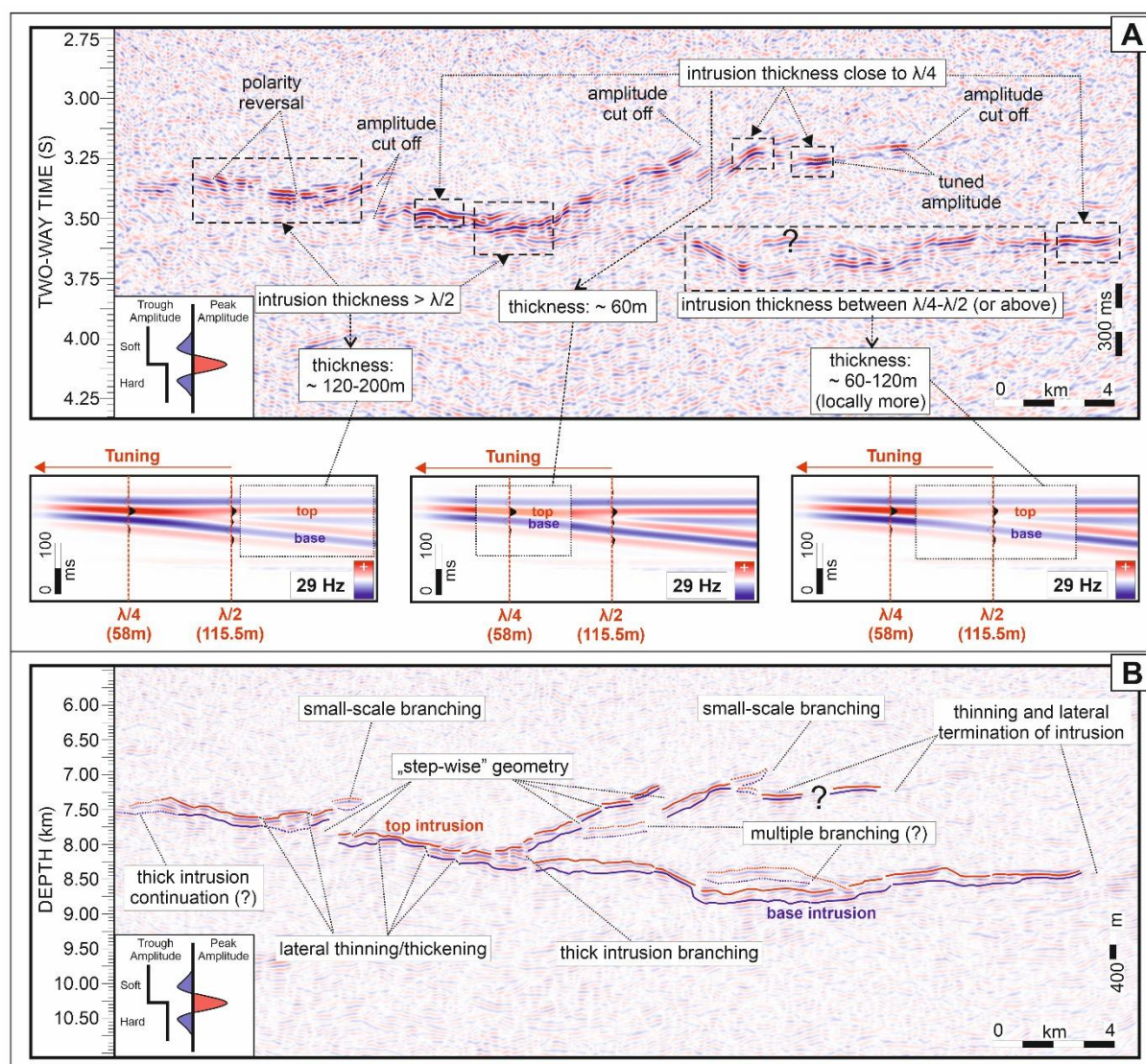
Figure 16: Seismic interpretation of igneous intrusion imaged by profile PL-1200 (cf. Fig. 8). (A) PreSTM seismic profile with
525 **detailed interpretation of reflection amplitude and an estimation of intrusion thickness based on seismic tuning and vertical**
resolution criteria obtained from the wedge model analysis (Fig. 13). Three wedge models, calculated using zero-phase Ricker
wavelet with 29 Hz dominant frequency, demonstrate various seismic responses depending on different sill thicknesses; (B) Part of
PreSDM PL-1200 profile that illustrates interpreted top and base of the intrusion and its inferred geometry.

530 **5 Discussion and conclusions**

In this study, we attempted to provide some "educated guesses" on possible interpretation of deep seismic features imaged by

PolandSPAN® regional deep seismic reflection data within the crystalline basement of the Baltic Basin in northern Poland.

These strong amplitude, semi-continues, locally divergent and partly saucer-shaped seismic reflectors are located at depths ranging from 6-7 to 19-20 km, are laterally extensive and continue for 100+ km. They were interpreted as seismic manifestation

535 of igneous intrusions. Since their depths are far beyond the reach of the deepest well, neither their lithology, nor thickness nor age could be unequivocally established. Nonetheless, these key elements of their characteristics could be determined with a reasonable degree of confidence by the constraints based on results of seismic forward modelling studies and regional geological context. Lithology was determined as dolerite, their thickness seems to be ranging from few tens of meters to 200 meters and more, and their age is most probably early Carboniferous.

540 Since the geological evolution of the studied part of the EEC is fairly well recognized thanks to numerous deep boreholes, phases of igneous activity in the study area and its broad vicinity are also fairly well known. Igneous intrusions known from this area could be related to one of these phases: (1) Mesoproterozoic (Calymmian) anorogenic igneous activity at c. 1.54 to 1.45 Ga, resulting in the development of the AMCG suite (Skridlaite et al., 2003; Krzemińska and Krzemiński, 2017), (2) late Ediacaran (c. 580-545 Ma) development of flood basalts of the Volhynia Large Igneous Province (Shumlyanskyy et al., 2016;

545 Poprawa et al., 2020; Krzemińska et al., 2022), (4) Mississippian alkaline magmatism in the Lublin-Baltic Large Igneous Province (c. 352–344 Ma; Poprawa et al., 2024; Krzemińska et al., 2025), and (4) calk-alkaline latest Carboniferous to early Permian magmatism (Breitkreuz et al., 2007; Maliszewska et al., 2016; Krzemińska et al., 2021b).

Association of analysed intrusions with the late Ediacaran and Permo-Carboniferous magmatism is unlikely, since the nearest proven appearances of their products are located at least 200 km away from the study area (Timmerman, 2004; Heeremanset

550 al., 2004; Maliszewska et al., 2016). Analyzed intrusions cross-cut both the Calymmian plutonic rocks as well as their Paleoproterozoic host rock, therefore, they must be younger than at least the main phase of the AMGC suite development. Moreover, dolerite intrusions are not known from the AMCG suite. Finally, similar extensive igneous intrusions have been imaged by the PolandSPAN® data also within the Silurian to Lower Devonian sedimentary cover of the Lublin Basin (Fig. 1) where they are known to be of an early Carboniferous age (Krzywiec et al., 2024; Poprawa et al., 2024). So, if these two

555 systems of intrusions from the Baltic and Lublin basins are genetically connected - which indeed seems very probable - then they both are younger than Early Devonian.

Taking all these facts into account, we postulate that an extensive system of intrusions imaged by PolandSPAN® seismic data in the deep crystalline basement of the Baltic Basin is of the Mississippian age, as suggested earlier by Mężyk et al. (2019). Several additional arguments could be brought to support such dating. Firstly, their location closely coincides with the shallow

560 intrusions of the Mississippian age, encountered in wells from the Baltic Basin, including also Pasłęk IG-1 deep research well that calibrated PL-1200 and PL-5400 seismic profiles (cf. Motuza et al., 2015; Poprawa et al., 2024). Those intrusions drilled by wells are built of dolerites which is coherent with the lithology of deep intrusions derived from seismic modelling described in this paper. Finally, deep intrusions imaged by seismic data are located in relatively close vicinity of a few igneous massifs in the western part of the Mazury High (Fig. 1B), also dated as Mississippian and being part of the LBMIP (Krzemińska et al.,

565 2025). All this rather unambiguously points to the Mississippian age of deep intrusions analysed in this paper.

Our methodology based on combined analysis of regional geological context, seismic data interpretation and detailed seismic modelling study proved to be very useful for "educated guessing" of deep igneous intrusions located beyond the reach of wells, and could be universally applied for similar studies elsewhere. It however should be remembered that it does rely on several assumptions so results should be treated with some degree of caution.

570

Acknowledgements

PolandSPAN® data used in this study was provided by ION Geophysical, and is acknowledged with many thanks. S&P Global kindly provided academic license of IHS Markit Kingdom seismic interpretation software. This study was supported by NCN grant UMO-2021/41/B/ST10/03550. PK and ŁS thank Joe Cartwright (Univ. of Oxford) for inspiring discussions on the early results of the study.

575

References

Andersson, U.B., Neymark, L. A., and Billström K.: Petrogenesis of Mesoproterozoic (Subjotnian) rapakivi complexes of central Sweden: implications from U–Pb zircon ages, Nd, Sr and Pb isotopes, Earth and Environmental Science Transactions of the Royal Society of Edinburgh, 92, pp 201-228, https://doi.org/10.1017/S0263593300000237, 2001.

Areń, B. and Lendzion, K.: Stratigraphic and lithologic characteristics of the Vendian and Lower Cambrian. Prace Instytutu Geologicznego, 90, 7–46, 1978 (in Polish with English summary).

Berthelsen, A.: Mobile Europe, in: A Continent Revealed – the European Geotraverse, edited by: Blundell, D. J., Freeman, R., and Mueller, S., Cambridge Univ. Press. 11–32, 1992.

Bjørlykke, K.: Compaction of Sedimentary Rocks Including Shales, Sandstones and Carbonates. In: Petroleum Geoscience: From Sedimentary Environments to Rock Physics, edited by: Bjørlykke, K., Springer, Berlin, Heidelberg, pp. 351–360, https://doi.org/10.1007/978-3-642-34132-8_13, 2015.

Bogdanova, S. V., Pashkevich, I. K., Gorbatschev, R., and Orlyuk, M. I.: Riphean rifting and major Palaeoproterozoic crustal boundaries in the basement of the East European Craton: geology and geophysics, Tectonophysics, 268, 1–21, https://doi.org/10.1016/S0040-1951(96)00232-6, 1996.

Bogdanova, S. V., Bingen, B., Gorbatschev, R., Kheraskova, T. N., Kozlov, V. I., Puchkov, V. N., and Volozh, Y. A.: The East European Craton (Baltica) before and during the assembly of Rodinia. Precambr. Res. 160 (1-2), 23–45, https://doi.org/10.1016/j.precamres.2007.04.024, 2008.

Breitkreuz, C., Kennedy, A., Geissler, M., Ehling, B.-C., Kopp, J., Muszyński, A., Protas, A., and Stouge, S:. Far Eastern Avalonia: Its chronostratigraphic structure revealed by SHRIMP zircon ages from Upper Carboniferous to Lower Permian

580

585

590

595

volcanic rocks (drill cores from Germany, Poland and Denmark), in: The Evolution of the Rheic Ocean: From Avalonian-Cadomian Active Margin to Alleghenian-Variscan Collision, edited by: Linnemann, U., Nance, R. D., Kraft, P., Zulauf, G., Geological Society of America, Special Paper, 423, 173–190, 2007.

Brown, A. R.: Structural Interpretation, in: Interpretation of Three-Dimensional Seismic Data, Seventh edition, edited by: Brown A. R., Investigations in Geophysics, Society of Exploration Geophysicists, 61-102, https://doi.org/10.1190/1.9781560802884.ch3, 2011.

Brown, LD. and Kim D.: Extensive Sills in the Continental Basement from Deep Seismic Reflection Profiling. Geosciences, 10, 449, https://doi.org/10.3390/geosciences10110449, 2020.

Burgess, S. D., Muirhead, J. D., and Bowring, S. A.: Initial pulse of Siberian Traps sills as the trigger of the end-Permian mass extinction. Nature Communications, 8(1), 1-6, https://doi.org/10.1038/s41467-017-00083-9, 2017.

Cartwright, J. and Hansen, D.: Magma transport through the crust via interconnected sill complexes, Geology, 34(11), 929–932, 2006.

Cartwright, J. and Huuse, M.: 3D seismic technology: the geological "Hubble.", Basin Research 17, 1–20, https://doi.org/10.1111/j.1365-2117.2005.00252.x, 2005

Cartwright, J., Foschi, M., and Philips, D.: The role of sill intrusion in delimiting the lateral propagation of giant dyke swarms: emplacement of the Dogger Sill Complex, Southern North Sea. Journal of Geological Society, 182, https://doi.org/10.1144/jgs2025-005, 2025.

Dadlez, R. and Marek, S.: Development of Permian and Mesozoic basins, in: Epicontinental Permian and Mesozoic in Poland, edited by: Marek, S. and Pajchlowa, M., Prace Państwowego Instytutu Geologicznego, 153, 403–409, 1997 (in Polish with English summary).

Demaiffe, D., Wiszniewska, J., Krzemińska, E., Williams, I. S., Stein, H., Brassinnes, S., Ohnenstetter, D., and Deloule, E.: A hidden alkaline and carbonatite province of early carboniferous age in Northeast Poland: Zircon U-Pb and pyrrhotite Re-Os geochronology, Journal of Geology, 121, 91–104, https://doi.org/10.1086/668674, 2013.

Domańska-Siuda, J., Grabarczyk-Gurba. A., and Nejbert, K.: Petrogenesis of microgranular enclaves in the A-type granitoid Krasnopol intrusion (Mazury Complex, northeastern Poland): Evidence of magma mixing, Mineralogy and Petrology, 118, 401–426, https://doi.org/10.1007/s00710-024-00866-1, 2024.

Domeier, M.: A plate tectonic scenario for the Iapetus and Rheic Oceans. Gondwana Research, 36, 275–295, https://doi.org/10.1016/j.gr.2015.08.003, 2016.

Dortman, N.B and Magid, M.Sh.: New data on velocity of elastic waves in crystalline rocks as a function of moisture. International Geology Review, 11 (5), 517-523., 1969.

Dowdell, B.L.: PySeisTuned2.0: https://www.pyseistuned.com/, last access: 3 February 2025, 2020.

Eide, C.H., Schofield, N., Lecomte, I., Buckley, S.J., and Howell, J.A.: Seismic interpretation of sill complexes in sedimentary basins: implications for the sub-sill imaging problem, J. Geol. Soc. 175, 193–209, https://doi.org/10.1144/jgs2017-096, 2017.

630   Eriksson, M.: Stratigraphy, facies and depositional history of the Colonus Shale Trough, Skåne, southern Sweden, Department of Geology, Lund University, Lund, 35 pp., 2012.

Fagin, S.W. (Ed): Seismic Modeling of Geologic Structures: Applications to Exploration Problems. Geophysical Development Series, Society of Exploration Geophysicists, pp. 1–267, 1991.

Faleide, T., Braathen A., Lecomte, I., Mulrooney, M., Midtkandal, I., Bugge, A., and Planke, S.: Impacts of seismic resolution
635   on fault interpretation: Insights from seismic modelling, Tectonophysics, 816, 229008, https://doi.org/10.1016/j.tecto.2021.229008, 2021.

Gaál, G. and Gorbatschev, R.: An Outline of the Precambrian Evolution of the Baltic Shield. Precambr. Res., 35, 15–52, 1987.

Gardner, G.H.F., Gardner, L.W., and Gregory, A.: Formation velocity and density—the diagnostic basics for stratigraphic traps, Geophysics, 39(6), 770-780, 1974.

640   Gorbatschev, R. and Bogdanova, S.: Frontiers in the Baltic Shield, Precambrian Research, 64, 3–21, https://doi.org/10.1016/0301-9268(93)90066-B, 1993.

Grabarczyk, A., Wiszniewska, J., Krzemińska, E., and Petecki, Z.: A new A-type granitoid occurrence in southernmost Fennoscandia: geochemistry, age and origin of rapakivi-type quartz monzonite from the Pietkowo IG1 borehole, NE Poland, Mineralogy and Petrology, 117, 1–25, https://doi.org/10.1007/s00710-022-00799-7, 2023.

645   Grad, M., Polkowski, M., and Ostaficzuk, S. R.: High resolution 3D seismic model of the crustal and uppermost mantle structure in Poland, Tectonophysics, 666, 188–210, https://doi.org/10.1016/J.TECTO.2015.10.022, 2016.

Hansen, D.M., Cartwright, J.A., Thomas, D.: 3D seismic analysis of the geometry of igneous sills and sill junction relationships, In: 3D Seismic Technology: Application to the Exploration of Sedimentary Basins, edited by Davies, R.J., Cartwright, J.A., Stewart, S.A., Lappin, M., Underhill, J.R., Geological Society, London, Memoir 29, 199–208, 2004.

650   Hansen, D.M. and Cartwright, J.: Saucer-shaped sill with lobate morphology revealed by 3D seismic data: implications for resolving a shallow-level sill emplacement mechanism, Journal of the Geological Society, London, 163, 2006, 509–523, 2006.

Hansen, D.M., Redfern, J., Federici F., di Biase D., Bertozzi G.: Miocene igneous activity in the Northern Subbasin, offshore Senegal, NW Africa, Marine and Petroleum Geology 25, 1–15, https://doi.org/10.1016/j.marpetgeo.2007.04.007, 2008.

655   Heeremans, M., Faleide, J. I., and Larsen, B. T.: Late Carboniferous-Permian of NW Europe: An introduction to a new regional map, in: Permo-Carboniferous Magmatism and Rifting in Europe, edited by: Wilson, M., Neumann, E.-R., Davies, G. R., Timmerman, M. J., Heeremans, M., and Larsen, B. T., Geological Society of London, vol. 223, pp 75–88, https://doi.org/10.1144/GSL.SP.2004.223.01.04, 2004.

Infante-Paez, L., and Marfurt, K.: In-context interpretation: Avoiding pitfalls in misidentification of igneous bodies in seismic
660   data, Interpretation, 6(4), SL29–SL42, http://dx.doi.org/10.1190/INT-2018-0076.1, 2018.

Jaworowski, K.: Depositional environments of the Lower and Middle Cambrian sandstone bodies. Biuletyn Państwowego Instytutu Geologicznego, 377: 1–118, 1997.

Johansson, Å., Bingen, B., Huhma, H., Waight, T., Vestergaard, R., Soesoo, A., Skridlaite, G., Krzeminska, E., Shumlyanskyy, L., Holland, M. E., Holm-Denoma, C., Teixeira, W., Faleiros, F. M., Ribeiro, B. V., Jacobs, J., Wang, C., Thomas, R. J.,
665   Macey, P. H., Kirkland, C. L., Hartnady, M. I. H., Eglington, B. M., Puetz, S. J., Condie, K. C.: A geochronological review of magmatism along the external margin of Columbia and in the Grenville-age orogens forming the core of Rodinia, Precambrian Research, 371, 106463, https://doi.org/10.1016/j.precamres.2021.106463, 2022.

Juhlin, C.: Interpretation of the reflections in the Siljan Ring area based on results from the Gravberg-1 borehole, Tectonophysics, 173, 345-360, 1990.

670   Juhlin, C., Sturkell, E., Ebbestad, J.O.R., Lehnert, O, Högström, A.E.S., Meinhold, G.: A new interpretation of the sedimentary cover in the western Siljan Ring area, central Sweden, based on seismic data, Tectonophysics 580, 88–99, http://dx.doi.org/10.1016/j.tecto.2012.08.040, 2012.

Juhlin, C., Hedin, P., Gee, D. G., Lorenz, H., Kalscheuer, T., and Yan, P.: Seismic imaging in the eastern Scandinavian Caledonides: siting the 2.5 km deep COSC-2 borehole, central Sweden, Solid Earth, 7, 769–787, https://doi.org/10.5194/se-
675   7-769-2016, 2016.

Kallweit, R.S. and Wood, L.C.: The limits of resolution of zero-phase wavelets. Geophysics 47, 1035–1046, https://doi.org/10.1190/1.1441367, 1982.

Kavanagh, J. L., and Sparks, R. S. J.: Insights of dyke emplacement mechanics from detailed 3D dyke thickness datasets. Journal of the Geological Society, 168(4), 965-978, https://doi.org/10.1144/0016-76492010-137, 2011.

680   Kheraskova, T. N., Volozh, Y. A., Antipov, M. P., Bykadorov, V. A., and Sapozhnikov, R. B.: Correlation of Late Precambrian and Paleozoic Events in the East European Platform and the Adjacent Paleooceanic Domains, Geotectonics, 49, 27–52, 2015.

Kiersnowski, H.: Depositional architecture of the Rotliegend Basin in Poland, Prace Państwowego Instytutu Geologicznego, 165: 113–128, 1998 (in Polish with English sum English summary).

685   Köpping, J., Magee, C., Cruden, A.R., Jackson, C.A.-L., and Norcliffe, J.R., , The building blocks of igneous sheet intrusions: Insights from 3-D seismic reflection data, Geosphere, 18(1), 156– 182, https://doi.org/10.1130/GES02390.1, 2022.

Krzemińska, E. and Krzemiński, L.: Geological map of crystalline basement in the Polish part of the East European Platform, 1 : 1 000 000, Polish Geological Institute–NRI, Ministry of Environment, Warsaw, 2017.

Krzemińska, E., Johansson, Å. E., Krzemiński, L., Wiszniewska, J., Williams, I. S., Petecki, Z., and Salwa, S.: Basement
690   correlation across the southernmost Baltic Sea: Geochemical and geochronological evidence from onshore and offshore deep drill cores, northern Poland, Precambrian Research, 362, 106300, https://doi.org/10.1016/j.precamres.2021.106300, 2021a.

Krzemińska, E., Krzemiński, L., Poprawa, P., Pacześna, J., and Nejbert, K.: First evidence of the post-Variscan magmatic pulse on the western edge of East European Craton: U-Pb geochronology and geochemistry of the dolerite in the Lublin
695   Podlasie basin, eastern Poland, Minerals, 11, 1361, https://doi.org/10.3390/min11121361, 2021b.

Krzemińska, E., Poprawa, P., Pacześna, J., and Krzemiński, L.: From initiation to termination: The evolution of the Ediacaran Volyn large igneous province (SW East European Craton) constrained by comparative geochemistry of proximal tuffs versus lavas and zircon geochronology, Precambrian Research, 370, 106560, https://doi.org/10.1016/j.precamres.2022.106560, 2022.

700 Krzemińska, E., Krzemiński, L., Demaiffe, D., Poprawa, P., Williams, I. S., and Wiszniewska, J.: Evidence of magmatic versus hydrothermal zircon ages and mantle-crust interactions obtained from the Carboniferous alkaline intrusions at the margin of East European Craton (NE Poland), Gondwana Research, 142: 44–72, https://doi.org/10.1016/j.gr.2025.01.017, 2025.

Królikowski, C. and Wybraniec, S.: Gravity and magnetic maps of Poland – historical background and modern presentation, Publications of the Institute of Geophysics, Polish Academy of Sciences, M18 (273), 87–92, 1996.

705 Krzywiec, P.: Structural inversion of the Pomeranian and Kuiavian segments of the Mid-Polish Trough – lateral variations in timing and structural style, Geological Quarterly, 51, 151–168, 2006.

Krzywiec ,P., Lis, P., Buffenmyer, V., Malinowski, M., and Lewandowski, M.: Regional Geologic Characterization of the Polish Lower Paleozoic Unconventional Play Using an Integrated Seismic and Well Data Approach, SPE AAPG SEG Unconventional Research Technology Conference, 12-14.08, Denver, Extended abstract, 5, 2013.

710 Krzywiec, P., Malinowski, M., Lis, P., Buffenmyer, V., Lewandowski, M.: Lower Paleozoic basins developed above the East European Craton in Poland: new insight from regional high-effort seismic reflection data. SPE/EAGE European Unconventional Resources Conference and Exhibition, Vienna (extended abstract, SPE-167739-MS), 2014.

Krzywiec, P., Gągała, Ł., Mazur, S., Słonka, Ł., Kufrasa, M., Malinowski, M., Pietsch, K., and Golonka, J.: Variscan deformation along the Teisseyre-Tornquist Zone in SE Poland: Thick-skinned structural inheritance or thin-skinned thrusting?, Tectonophysics, 718, 83–91, http://dx.doi.org/10.1016/j.tecto.2017.06.008, 2017a.

Krzywiec, P., Mazur, S., Gągała, Ł., Kufrasa, M., Lewandowski, M., Malinowski, M., and Buffenmyer, V., Late Carboniferous thin-skinned compressional deformation above the SW edge of the East European craton as revealed by seismic reflection and potential field data—Correlations with the Variscides and the Appalachians, in: Linkages and Feedbacks in Orogenic Systems, edited by: Law, R. D., Thigpen, J. R., Merschat, A. J., Stowell, H. H., Geological Society of America Memoir, 720 213, 353–372, https://doi.org/10.1130/2017.1213(14), 2017b.

Krzywiec, P., Poprawa, P., Mikołajczak, M., Mazur, S., and Malinowski, M.: Deeply concealed half-graben at the SW margin of the East European Craton (SE Poland) – Evidence for Neoproterozoic rifting prior to the break-up of Rodinia, Journal of Palaeogeography, 7 (1), 88-97, https://doi.org/10.1016/j.jop.2017.11.003, 2018.

Krzywiec, P., Kufrasa, M., Poprawa, P., Mazur, S., Koperska, M., and Ślemp, P.: Together but separate: decoupled Variscan 725 (late Carboniferous) and Alpine (Late Cretaceous – Paleogene) inversion tectonics in NW Poland, Solid Earth, 13, 639–658, https://doi.org/10.5194/se-13-639-2022, 2022.

Krzywiec, P., Słonka, Ł., and Poprawa, P.: Lower Carboniferous magmatic intrusions within the SW edge of the East European Craton (Baltic and Lublin basins, Poland) – Insight based on seismic data interpretation and seismic forward modelling,

SEISMIX 2024 - 20th International Symposium on Deep Seismic Profiling of the Continents and their Margins, Uppsala,
730 24-28.06, Abstract volume, 47, 2024.

Kufrasa M., Krzywiec P., Gągała Ł., Mazur S., and Mikołajczak M.: Sequence of deformation at the front of an orogen: Lublin basin case study (Poland). Journal of Structural Geology, 141, 104211; https://doi.org/10.1016/j.jsg.2020.104211, 2020.

Kuzmenkova, O. F., Nosova, A. A., and Shumlyanskyy, L. V.: 2010. Correlation of the Neoproterozoic Volyn-Brest magmatic province with large continental plateau basalt provinces of the world, nature of low- and high-titanium basite magmatism,
735 Litasfera, 2 (33), 3–16, 2010 (in Russian with English abstract).

Lazauskienė, J., Stephenson, R., Šliaupa, S., and Van Wees, J.-D.: 3-D flexural modelling of the Silurian Baltic Basin, Tectonophysics, 346, 115–135, https://doi.org/10.1016/S0040-1951(01)00231-1, 2002.

Lecomte I., Lavadera, P.L., Anell, I., Buckley, S.J., Schmid D.W., and Heeremans, M.: Ray-based seismic modeling of geologic models: Understanding and analyzing seismic images efficiently, Interpretation, 3(4) SAC71–SAC89,
740 http://dx.doi.org/10.1190/INT-2015-0061.1, 2015.

Li, J., and Mitra, S.: Seismic modeling and expression of common fold-thrust structures, Interpretation 8 (1), 1–39, 2020a.

Li, J., and Mitra, S.: Seismic models of detachment and faulted detachment folds. Marine and Petroleum Geology 117, 1-11, https://doi.org/10.1016/j.marpetgeo.2020.104385, 2020b.

Magee, C. and Jackson, C.A-L.: Seismic reflection data reveal the 3D structure of the newly discovered Exmouth Dyke Swarm,
745 offshore NW Australia, Solid Earth, 11, 579–606, https://doi.org/10.5194/se-11-579-2020, 2020.

Malinowski, M.: Deep reflection seismic imaging in SE Poland using extended correlation method applied to PolandSPANTM data, Tectonophysics, 689, 107–114, https://doi.org/10.1016/j.tecto.2016.01.007, 2016.

Maliszewska, A., Jackowicz, E., Kuberska, M., and Kiersnowski, H.: Lower Permian (Rotliegend) rocks of western Poland: a petrographic monograph, Prace Państwowego Instytutu Geologicznego, 204, 6–115, 2016 (in Polish with English
750 summary).

Matyja, H., Stratigraphy and facies development of the Devonian and Carboniferous in the Pomeranian Basin and western Balic Basin with relation to Palaeozoic palaeogeography of the northern TESZ, Prace Państwowego Instytutu Geologicznego, 186, 79–122, 2006 (in Polish with English summary).

Maystrenko Y.P., Bayer U., Brink H-J., and Littke R.: The Central European Basin System – an Overview, [in]: Littke R.,
755 Bayer U., Gajewski D., Nelskamp S., [eds.], Dynamics of complex intracontinental basins: The Central European Basin System: Springer Verlag, 17-34, 2008.

Mazur S., Mikołajczyk M., Krzywiec P., Malinowski M., Buffenmyer V., and Lewandowski M.: Is the Teisseyre-Tornquist Zone an ancient plate boundary of Baltica? Tectonics, 34(12): 2465–2477 http://doi.org/10.1002/2015TC003934, 2015.

Mazur S., Mikolajczak M., Krzywiec P., Malinowski M., Lewandowski M., and Buffenmyer V.: Pomeranian Caledonides,
760 NW Poland - a collisional suture or thin-skinned fold-and-thrust belt? Tectonophysics, 692: 29–43. https://10.1016/j.tecto.2016.06.017, 2016.

Mazur, S., Porębski, Sz. J., Kędzior, A., Paszkowski, M., Podhalańska, T., and Poprawa P.: Refined timing and kinematics for Baltica-Avalonia convergence based on the sedimentary record of foreland basin, Terra Nova, 30, 8–16, http://doi.org/10.1111/ter.12302, 2018.

765   McBride, J. H., White, R. SD., Smallwood, J. R., and England, R. W.: Must magmatic intrusion in the lower crust produce reflectivity?, Tectonophysics, 388, 271–297, 2004.

Mężyk, M., Malinowski, M., and Mazur, S.: Imaging the East European Craton margin in northern Poland using extended correlation processing of regional seismic reflection profiles, Solid Earth, 10, 683–696, https://doi.org/10.5194/se-10-683-2019, 2019.

770   Mężyk, M., Malinowski, M., Mazur, M.: Structure of a diffuse suture between Fennoscandia and Sarmatia in SE Poland based on interpretation of regional reflection seismic profiles supported by unsupervised clustering, Precambrian Research 358, 106176, https://doi.org/10.1016/j.precamres.2021.106176, 2021.

Miles, A. and Cartwright J.: Hybrid flow sills: A new mode of igneous sheet intrusion, Geology, 38(4), 343–346; https://doi.org/10.1130/G30414.1, 2010.

775   Modliński, Z.: The Development of Ordovician lithofacies and palaeotectonics in the area of the Precambrian Platform in Poland, Prace Instytutu Geologicznego, 52: 1–65, 1982, (in Polish with English summary).

Motuza, G., Šliaupa, S., and Timmerman, M. J.: Geochemistry and 40Ar/39Ar age of Early Carboniferous dolerite sills in the southern Baltic Sea, Est. J. Earth Sci., 64, 233, https://doi.org/10.3176/earth.2015.30, 2015.

Muirhead, J. D., Airoldi, G., Rowland, J. V., and White, J. D.: Interconnected sills and inclined sheet intrusions control shallow
780   magma transport in the Ferrar large igneous province, Antarctica. Geo. Soc. Am. Bull., 124(1-2), 162-180, https://doi.org/10.1130/B30455.1, 2012.

Murase, T. and McBirney, A. R.: Properties of some common igneous rocks and their melts at high temperatures. Geo. Soc. Am. Bull., 84, 3563–3592, 1973.

Neumann, E.-R., Wilson, M., Heeremans, M., Spencer, E. A., Obst, K., Timmerman, M. J., and Kirstein, L.: Carboniferous-
785   Permian rifting and magmatism in southern Scandinavia, the North Sea and northern Germany: A review, in: Permo-Carboniferous Magmatism and Rifting in Europe, edited by: Wilson, M., Neumann, E.-R., Davies, G. R., Timmerman, M. J., Heeremans, M., Larsen, B. T., Geological Society, Special Publications, London, 223, 11–40, 2004.

Pańczyk, M. and Nawrocki, J.: Tournaisian 40Ar/39Ar age for alkaline basalts from the Lublin Basin (SE Poland), Geological Quarterly, 59, 473–478, http://dx.doi.org/10.7306/gq.1218, 2015.

790   Papasikas, N. and Juhlin, C.: Interpretation of reflections from the central part of the Siljan Ring impact structure based on results from the Stenberg-1 borehole, Tectonophysics, 269, 237-245, 1997.

Peryt, T.M., Geluk, M.C., Mathiesen, A., Paul, J. and Smith, K.: Zechstein, in: Petroleum Geological Atlas of the Southern Permian Basin Area, edited by Doornenbal, J.C. and Stevenson, A.G., EAGE Publications b.v. (Houten): 123-147, 2010.

Petecki, Z. and Rosowiecka, O.: A new magnetic anomaly map of Poland and its contribution to the recognition of crystalline
795   basement rocks, Geological Quarterly, 61, 934–945, http://dx.doi.org/10.7306/gq.1383, 2017.

Piwocki, M. and Kramarska, R.: Polish Lowlands and their southern rim – basics of stratigraphy, in: Geological Setting of Poland, Vol. 1, Stratigraphy, Part 3a, Cenozoic, Paleogene, Neogene, edited by: Peryt, T. and Piwocki, M., Polish Geological Institute, Warsaw, 19–22, 2004 (in Polish with English summary).

Plewa, M. and Plewa, S.: Petrofizyka, Wydawnictwa Geologiczne, Warszawa, Poland, 327 pp., 1992 (in Polish).

800   Podhalańska, T. and Modliński, Z.: Stratigraphy and facies characteristics of the Ordovician and Silurian deposits of the Koszalin-Chojnice Zone; similarities and differences to the western margin of the East European Craton and the Rügen area. Prace Państwowego Instytutu Geologicznego, 186: 39–78, 2006 (in Polish with English summary).

Poprawa, P.: Geological setting and Ediacaran–Paleozoic evolution of the western slope of the East European Craton and adjacent regions, Annales Societatis Geologorum Poloniae, 89, 347–380, https://doi.org/10.14241/asgp.2019.23, 2019.

805   Poprawa, P.: Lower Paleozoic oil and gas shale in the Baltic-Podlasie-Lublin Basin (central and eastern Europe) – a review, Geological Quarterly, 64, 515–566, http://dx.doi.org/10.7306/gq.1542, 2020.

Poprawa, P., Šliaupa, S., Stephenson, R. A., and Lazauskiene, J.: Late Vendian-Early Palaeozoic tectonic evolution of the Baltic basin: regional implications from subsidence analysis, Tectonophysics 314, 219–239, https://doi.org/10.1016/S0040-1951(99)00245-0, 1999.

810   Poprawa, P., Radkovets, N., and Rauball, J.: Ediacaran-Paleozoic subsidence history of the Volyn-Podillya-Moldova basin (Western and SW Ukraine, Moldova, NE Romania), Geological Quarterly, 62, 459–486, https://doi.org/10.7306/gq.1418, 2018.

Poprawa, P., Krzemińska, E., Paceśna., J., and Amstrong, R.: Geochronology of the Volyn volcanic complex at the western slope of the East European Craton – relevance to the Neoproterozoic rifting and the break-up of Rodinia/Pannotia,

815   Precambrian Research, 346, 105817, https://doi.org/10.1016/j.precamres.2020.105817, 2020.

Poprawa, P., Nejbert, K., Krzywiec, P., Krzemińska, E., Krzemiński, L., Mazur, S., and Słaby, E.: Alkaline magmatism from the Lublin-Baltic area of Poland (SW slope of the East European Craton) – Manifestation of hitherto unrecognized early Carboniferous igneous province, Terra Nova, 36 (1), 77–88, doi:10.1111/ter.12681, 2024.

Porębski, S. J. and Podhalańska, T.: Ordovician–Silurian lithostratigraphy of the East European Craton in Poland, Annales

820   Societatis Geologorum Poloniae, 89: 95–104, doi: https://doi.org/10.14241/asgp.2019.05, 2019.

Rabbel, O., Galland, O., Mair, k., Lecomte, I., Senger, K., Spacapan, J.B., and Manceda, R.: From field analogues to realistic seismic modelling: a case study of an oil-producing andesitic sill complex in the Neuquén Basin, Argentina, Journal of the Geological Society, 175, 580 – 593, https://doi.org/10.1144/jgs2017-116, 2018.

Sheriff, R.E.: Encyclopedic Dictionary of Applied Geophysics, Fourth edition. Society of Exploration Geophysicists, Tulsa,

825   Oklahoma, pp. 442, https://doi.org/10.1190/1.9781560802969.chm, 2002.

Shumlyanskyy, L., Nosova, A., Billström, K., Söderlund, U., Andréasson, P.-G., and Kuzmenkova, O., The U-Pb zircon and baddeleyite ages of the Neoproterozoic Volyn Large Igneous Province: implication for the age of the magmatism and the nature of a crustal contaminant, Geol. Foeren. Stockholm Foerh., 138 (1), 17–30, http://dx.doi.org/10.1080/11035897.2015.1123289, 2016.

830   Shumlyanskyy, L., Belousova, E., and Petrenko, O.: Geochemistry of zircons from basic rocks of the Korosten anorthosite-mangerite-charnockite-granite complex, north-western region of the Ukrainian Shield, Mineralogy and Petrology, 111 (4), 459–466, https://doi.org/10.1007/s00710-017-0514-2, 2017.

Skridlaitė, G., Wiszniewska, J., Duchess, J-C.: Ferro-potassic A-type granites and related rocks in NE Poland and S Lithuania: west of the East European Craton, Precambrian Research, 124, 305–326, https://doi.org/10.1016/S0301-9268(03)00090-1,
835   2003.

Słonka, Ł., Krajewski, M., and Krzywiec, P.: Internal structure of the Upper Jurassic subsurface carbonate buildups of the northern Tethys shelf in southern Poland – integration of seismic forward modeling and outcrop analogs, Marine and Petroleum Geology, 177, 107367, https://doi.org/10.1016/j.marpetgeo.2025.107367, 2025.

Stachowska, A. and Krzywiec, P.: The Late Cretaceous tectono-sedimentary evolution of northern Poland – A seismic
840   perspective on the role of transverse and axial depositional systems during basin inversion, Marine and Petroleum Geology, 152, 106224, https://doi.org/10.1016/j.marpetgeo.2023.106224, 2023.

Tari, G., Poprawa, P., and Krzywiec, P.: Silurian Lithofacies and Paleogeography in Central and Eastern Europe: Implications for Shale Gas Exploration, SPE 151606, SPE/EAGE European Unconventional Resources Conference and Exhibition, Vienna, 20-22, 2012.

845   Timmerman M.J.: Timing, geodynamic setting and character of Permo-Carboniferous magmatism in the foreland of the Variscan Orogen, NW Europe, Geological Society, London, Special Publications, 223, 41–74, https://doi.org/10.1144/GSL.SP.2004.223.01.03, 2004.

Torsvik, T.H. and Rehnström, E.F.: The Tornquist Sea and Baltica–Avalonia docking, Tectonophysics, 362, 67–82, doi: 10.1016/S0040-1951(02)00631-5, 2003.

850   Wagner, R.: Stratigraphy and development of the Zechstein basin in the Polish Lowlands, Prace Państwowego Instytutu Geologicznego, 146, 1–71, 1994 (in Polish with English summary).

Widess, M.B.: How thin is a thin bed? Geophysics, 38, 1176–1180, 1973.

Wiszniewska, J., Petecki, Z., Krzemińska, E., Grabarczyk, A., and Demaiffe, D.: The Tajno ultra mafic-alkaline- carbonatite massif, NE Poland: A review. Geophysics, petrology, geochronology and isotopic signature, Geological Quarterly, 64,
855   402–421, https://doi.org/10.7306/gq.1535, 2020.

Wrona, T., Magee, C., Fossen, H., Gawthorpe, R.L., Bellw, R.E, Jackson, C.A.-L, and Faleide, J.I.: 3-D seismic images of an extensive igneous sill in the lower crust, Geology, 47, 729–733, https://doi.org/10.1130/G46150.1, 2019.

Wybraniec, S.: Transformations and visualization of potential field data, Polish Geological Institute Special Papers, 1, 1–28, 1999.

860   Zeng, H., Loucks, R.G., and Reed, R.M.: Three-dimensional seismic architecture of an Upper Cretaceous volcanic complex and associated carbonate systems; Taylor Group, Elaine field, South Texas, USA, Marine and Petroleum Geology 155, 106350, https://doi.org/10.1016/j.marpetgeo.2023.106350, 2023.